APPLICATIONS OF LASER MICROBEAM IN THE STUDY OF DEGENERATION, REGENERATION, AND GUIDANCE OF PRIMARY CNS AXONS

by

BRYAN JAMES BLACK

Presented to the Faculty of the Graduate School of

The University of Texas at Arlington in Partial Fulfillment

of the Requirements

for the Degree of

MASTER OF SCIENCE IN PHYSICS

THE UNIVERSITY OF TEXAS AT ARLINGTON

December 2012

Acknowledgements

First, I need to thank my research advisor, Dr. Samarendra Mohanty, for the scientific ideals and confidence he has instilled in me, as well as the opportunities he has afforded me. When I joined the biophysics and physiology lab at UTA, I had absolutely no prior research experience and zero expertise. In spite of that, he showed interest in my development and ultimately entrusted me with projects and responsibilities that I have not deserved. His passion and optimism for our group's research constantly astound me, and his example will always serve as my standard.

I would like to thank Dr. Ling Gu for her assistance in cell culture, as well as her advice and insight concerning all things 'biology.' I would also like to thank the members of the biophysics and physiology lab at UTA for their ongoing input, encouragement, and support. Specifically, I need to thank Simon Ordonez for his assistance in cell culture and goldfish retinal explant derivation.

I would like to thank Dr. Kim and Dr. Koymen for agreeing to serve on my thesis defense committee.

Thanks to Dr. Kim and his lab group for providing rat cortical neurons for optical guidance experiments, and thanks to Dr. Mondal for his collaboration in estrogen experiments.

My family has also been instrumental in my education (and my life, general). They have encouraged me, in word and example, to never stop learning. They have lived their lives with a dignity, intelligence and fortitude that I will always aspire to. Thank you.

Finally, I would like to thank my wife, Erica Hutchins Black, who has sacrificed more for the sake of my education than anyone else. She has tolerated more than I would ever consciously ask of her. She has given more than I could ever return. So this

thesis belongs to her, as well as any subsequent degrees, diplomas, awards, certifications, commendations, pay, and/or atta-boys that I should receive between now and the time that I leave this earth. My written and verbal thanks will always seem grossly insufficient, so I thank her by writing this thesis; by finishing what I started out to do, and by doing it as well as I know how. Thank you.

November 19th, 2012

Abstract

APPLICATIONS OF LASER MICROBEAM IN THE STUDY OF DEGENERATION, REGENERATION, AND GUIDANCE OF PRIMARY CNS AXONS

Bryan James Black

The University of Texas at Arlington, 2012

Supervising Professor: Samarendra Mohanty

This thesis explores the applications of a near infrared (NIR) laser microbeam as a tool for manipulating primary axons by initiating femtosecond pulsed-laser plasma-mediated ablation (laser axotomy) and optical guidance. Chapter 1 briefly introduces axon morphology, growth, and the principles of axon guidance, as well as an introduction to the unique capabilities/potential provided by laser microbeams in biological research (laser-tissue interactions). Non-linear, multiphoton absorption processes are discussed in context of biological tissue ablation. In addition, we discuss specific challenges facing mammalian central nervous system (CNS) axons subsequent to injury, and comment on strategies which can be employed to mitigate, remove, or circumvent those challenges using neuroprotective factors and NIR laser microbeam.

With a basic understanding of laser-tissue interaction, Chapter 2 presents results on degeneration and regeneration dynamics of retinal ganglion cell (RGC) axons subsequent to varying degrees of fs laser-induced injury. Axons were damaged using three distinct sets of parameters, resulting in three reproducibly distinct initial injuries (all resulting in complete axotomy). Regeneration rates and pathfinding abilities were shown to decrease in axons suffering higher degree of initial injury. Chapter 2 also presents results of degeneration and regeneration dynamics subsequent to fs laser axotomy in the

presence and absence of estrogen, which has been shown to mitigate degenerative effects and is implicated in successful regeneration of CNS axons.

Chapter 3 presents a novel, purely optical method to guide the growth of primary CNS axons that uses a low power, near infrared laser microbeam. This non-contact method is highly efficient in realizing large turning angles and is 100% effective. Optical guidance is successfully applied to primary RGC, as well as rat cortical neuron (RCN) axons. Possible mechanisms of guidance are discussed and analyzed using optical force (photomechanical) and local temperature rise (photothermal) simulations. This method is minimally invasive and is adaptable to fiber-optics, illustrating exciting potential as a method of bypassing CNS glial scar formations, which are major inhibitory factors in CNS nerve repair. Applications of optical guidance to spinal cord injury repair and neural circuitry formation are discussed in detail, as is the future direction of our research (Chapter 4).

Table of Contents

List of Illustrations

Chapter 1

Introduction

1.1 Brief introduction and justification

Emerson Pugh once said that “If the human brain were so simple that we could understand it, we would be so simple that we couldn’t” [1]. There are some days I think he was right. The human brain contains billions of cells (neurons), sharing far more than a trillion connections between them. But for all of the fantastic, mysterious capabilities attributable to our central nervous system (CNS), it cannot repair and regenerate, unlike our peripheral nervous system. That is the central reason that CNS injury and disorder in humans is so catastrophic. There is little possibility of recovery of lost function after the onset of disease or injury. This has tremendous implications in terms of the millions of people affected by stroke, traumatic brain injury, spinal cord injury, Parkinson’s disease, Alzheimer’s disease, glaucoma, etc. So why don’t mature mammalian CNS neurons, like RGCs, regenerate their axons following injury? Is there a way to mitigate the injury response in a way that limits the damage and results in successful mammalian CNS regeneration? And, perhaps most importantly, if we can get these nerves to regenerate, how do we effectively guide them *in vivo* to regions that will result in the reformation of functional connections?

Since that quote was published, more than thirty years ago, tremendous strides have been made in understanding neural function, development, and injury. Advances in analytic systems and imaging platforms have given us new insight into the molecular and physical forces at work in developmental and regenerative neurology. Spinal cord injury is no longer a problem that we trying to contain, but correct. However, future investigation and treatment of spinal cord injury requires the further development of non-

invasive diagnostic, analytic and therapeutic tools. These tools should be minimally invasive, have a high spatial and temporal resolution, and maximum efficiency.

Using wavelengths in the near infrared (NIR) to infrared (IR) regime, light has shown uniquely promising capabilities in the manipulation and analysis of biological objects in a non-damaging and efficient manner. For these reasons, light has gained considerable interest as a possibly ideal tool for implementing research and therapeutic programs targeted at *in vivo* CNS nerve repair.

1.2 Axon morphology, growth and guidance

An axon is the outgoing communication pathway of a neuron. It is a protrusion that extends outward, away from the cell body, with the purpose of creating a physically stable and functionally connected neural network in cooperation with other neurons (Figure 1:1). The common morphological analogy is to visualize the axon as your arm and hand. Your arm is the axon shaft, extending away from your body, containing an internal skeleton and circulatory system (cytoskeleton and microtubules), which serve as support structures for the skin (the plasma membrane), and transport pathways to your hand. Within the axon shaft, the cytoskeleton consists largely of parallel microtubules, bundled together, oriented with their 'positive' ends directed towards the growth cone. These bundled microtubules act as transportation tracks for the kinesin and dynein molecular motors, which actively carry membrane vesicles either retrograde (back toward the cell body), or anterograde (toward the growth cone).

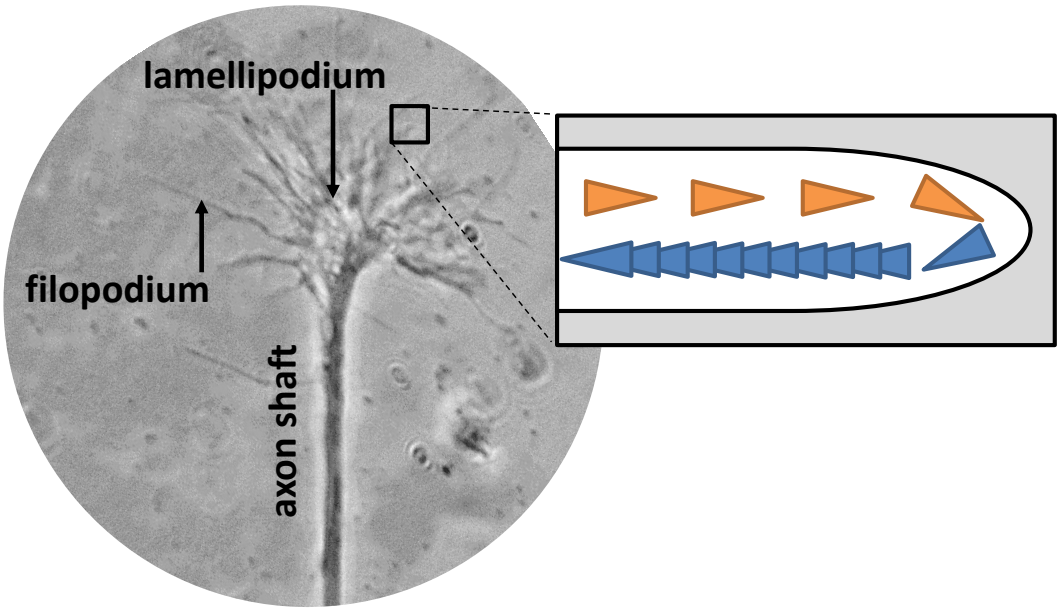

Figure 1:1 Basic morphology of axon shaft (distal end) and growth cone. The zoomed area illustrates the principle of actin treadmill at work within filopodia.

You can think of your hand as the growth cone, which is a highly motile structure that is able to sense environmental cues and direct the axon along paths that will result in a stable and functional neural network. The growth cone is tipped with finger-like protrusions, called filopodia. Filopodia are also highly motile sensing structures, which can react to the environment independently from the growth cone, and even independently of one another [2]. As the growth cone crawls along within the developing or regenerating nervous system, it trails the axon shaft behind it. Thus, it is the growth cone that largely determines the final trajectory of an axon, although subsequent straightening or collateral branching can occur (your hand can only go where your arm can follow).

Growth cones undergo constant structural change. This morphological change is a result of the constant deconstruction and reconstruction of the internal actin network; a process which is sometimes referred to as the 'actin treadmill.' Unpolymerized g-actin

(globular actin) diffuses outward into the peripheral regions of the growth cone and preferentially polymerizes near the cell membrane, where it becomes f-actin (filamentous actin). The polymerized actin network is then drawn toward the central region of the growth cone by myosin, where it undergoes depolymerization. It is this process, repeated over and again which is thought to generate traction between the axon membrane and a permissive substrate via adhesion molecules. When the actin-based tread gets a grip on the substratum, it can advance the leading edge of the growth cone and draws it forward. An axon's growth is typically capricious, with periods of fast growth interrupted by periods of slow (or no) growth. The advancement behavior of the growth cone is modulated as it encounters stimuli in the environment. These changes in directional behavior (*in vivo*) often occur at what have been called "decision points," where growth cone chooses between alternate pathways [3].

An axon's advancement is not random, but highly biased by environmental guidance cues. These cues are primarily chemical in nature, but can also include force (fluid flow) and temperature gradients. Growth cones sense these environmental guidance cues and respond by growing selectively toward or away from them, depending on whether the guidance cue is attractive or repulsive. Calcium and cyclic nucleotides (cAMP and cGMP) have been highly implicated in this process, with the relative concentrations of these molecules within the growth cone effectively changing the polarization of the external guidance cue from attractive to repulsive or vice versa. Furthermore, channels along the membrane can be chemically, mechanically, electrically, and thermally activated to allow for the influx of extracellular ions (ie calcium) into individual filopodia or localized regions of the growth cone. Calcium influx is known to lead to localized depolymerization of the actin network, and can therefore arrest the polymerization and outgrowth process.

The growth cone is also a highly polarized dynamical structure, and advances only at its leading edge. Its ability to make sharp turns (>90 degrees) is limited by this extreme polarization. Since there are often multiple guidance cues in the environment, often at very small gradients, integration and amplification of external signals are also fundamental functions of the growth cone. While peripheral nerves (axons) are known to regenerate subsequent to axotomy, mammalian CNS nerves do not regenerate *in vivo*. While this was once thought to be an intrinsic quality of CNS neurons, it has been shown that inhibitory environmental factors play a significant role in suppressing CNS nerve repair.

1.3 Challenges to CNS (spinal cord) repair

Every year, more than 10,000 individuals sustain spinal cord injuries in the United States. Spinal cord injuries cause compression, contusion, penetration and maceration of central nervous system tissue that results in death of neurons and destruction of axonal connections [4], with only a small percentage of injured patients recovering from sever functional impairment. For many years, it was thought that CNS axons, unlike those of the peripheral nervous system (PNS), did not have the inherent capacity to regenerate [5]. However, it was first shown that CNS axons had the ability to regenerate into peripheral nerve grafts [6] in 1980. These findings suggested that the failure to regenerate may not be an inherent deficiency of CNS axons, but that they are inhibited by external environmental factors. Since then, it has been established that there are both extrinsic and intrinsic factors that prevent CNS axons from repair.

Studies in this area have demonstrated that injury to the spinal cord involves an acute damage phase followed by a long-lasting period of secondary degeneration. During the acute phase, mechanical stretching and shearing damage neurons and their surrounding vasculature, forming what has been called the primary lesion [7, 8, 9].

During the secondary degeneration phase, which occurs in the days, weeks and months following the primary injury, axons degenerate away from the site of injury and additional death of neurons and glia leads to a progressive enlargement of the primary lesion site [10].

Further complications are caused by a massive inflammatory response to CNS injury [11]. In general, inflammation in the CNS is triggered by resident microglia in the vicinity of the lesion that are activated in response to tissue disruption and vascular damage during the primary injury stage [12, 13, 14]. Microglia secrete pro-inflammatory cytokines that recruit additional immune cells, including neutrophils and monocytes, to the lesion site. Spinal cord damage is amplified when immune cells secrete neurotoxic factors and produce reactive oxygen species during phagocytosis. Cell death and membrane damage caused by these factors likely contributes to secondary degeneration [11]. Secondary degeneration due to inflammation and other factors is eventually attenuated by formation of a glial scar [15]. During this process, activated astrocytes act in concert with several other cell types to establish a physical barrier surrounding the lesion site [16]. In fact, wherever the CNS is damaged, a glial scar forms. This scarring is first evident within hours of injury and develops further over a period of weeks. This, together with chemically toxic factors, leads to a highly inhibitory extracellular matrix through which axons would have to regenerate.

CNS regeneration and pathfinding failure represents a formidable barrier to recovery and consequently, no treatments currently exist for repairing spinal cord injury. Instead, post-injury care for SCI is limited to procedures aimed at minimizing cord damage that can occur after the initial injury. A number of strategies for promoting axon regeneration have now been tested, including neutralizing myelin inhibitors, degrading

inhibitory ECM molecules, providing growth substrates within lesion sites, and treatment with growth-promoting/degeneration-reducing factors.

1.4 Estrogen as a neuroprotective

Estrogen is an important hormone which is found in humans and regulates multiple functions in the body. Classically, estrogen is considered a "reproductive" hormone, due to its well-known role in feedback signaling in the hypothalamic-pituitary-ovarian axis. The consideration of estrogen's neuroprotective benefits was, in part, sparked by the well known sex differences in risk, onset and severity of neurodegenerative diseases (e.g. Alzheimer's disease, Parkinson's disease and stroke). Indirect scientific evidence that estrogen may be neuroprotective first arose from studies of such sex differences following brain injuries in animals [17]. For example, female rats have been reported to have greater survival rates as compared to males following diffuse traumatic brain injury [18]. A number of studies have documented that women are "protected" against stroke relative to men – at least until the years of menopause, when estrogen levels decline [19, 20, 21]. In addition to a potential direct protective action on neurons, there is evidence that estrogen may also have indirect effects on other cell types such as astrocytes and microglia that may facilitate its neuroprotective action in cerebral ischemia and other neurodegenerative disorders [22, 23, 24]. After neuronal injury and in many neurodegenerative disorders, activated microglia are known to secrete proinflammatory factors that can contribute to the progressive neural damage. A number of studies have suggested that estrogen may act upon microglia to suppress their activation, an effect that could help mediate estrogen neuroprotection [25, 26].

1.5 Laser microbeam as biomedical tool

1.5.1 Optical forces

Over the past 25 years, laser microbeams have been employed to optically trap, stretch, analyze, and surgically dissect biological samples ranging from whole cells to internal cell structures down to single DNA molecules. Safely probing biological samples with laser irradiation requires that the incident light's wavelength be independent of the sample material's linear absorption coefficient [27]. While biological macromolecules are known to strongly absorb wavelengths in the ultraviolet (200-400nm) regime, severely limiting the possible usage of UV wavelengths in deep tissue studies [28], they are (semi-) transparent to near-infrared (NIR) wavelengths (~800nm), and the laser light can be focused beyond collateral cellular structures and focused within a region of interest without significantly disturbing biological material above or below the laser focal spot. Only if the laser microbeam is tightly focused and operated at or above a threshold power, will biological material be laser-pulse ablated (a process that will be discussed in detail later on in this section) using NIR light.

When an optical beam is incident on an interface, the beam is deflected from its original path due to reflection and/or refraction. This deflection represents changes in the momenta of single photons translating along the path of the beam, and these momentum changes give rise to optical forces, acting on the deflecting object. These optical forces can be classified into two types, the scattering force and the gradient force [29].

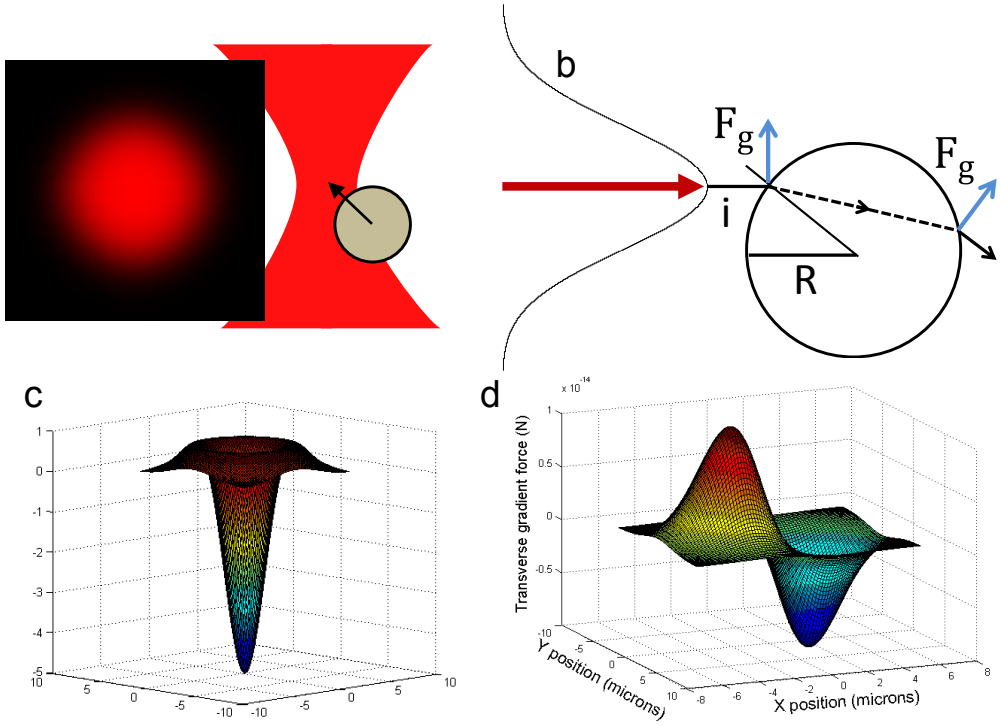

Figure 1:2 (a) Illustration of a Gaussian beam intensity cross section and side view of dielectric sphere being drawn towards Gaussian laser beam waist. (b) Description of optical gradient force vectors acting on dielectric sphere of radius R. (c) Illustration of characteristic z direction gradient force magnitude (direction of light propagation) in the Rayleigh regime. (d) Illustration of characteristic x-direction gradient force magnitude acting on dielectric sphere (Rayleigh regime)

The scattering force is mostly a result of the reflection at the interface, but is also due to scattering and absorption of incident photons. The scattering force is always acting along the direction of the propagating beam. The gradient force is along both the transverse and axial directions of the laser beam, and it pulls the object towards the position of highest intensity, which is tantamount to an optical equilibrium position, so that any displacement from this position will result in a restoring force, just like a spring, but in

three dimensions. There is a general size limitation to the types of objects which can be effectively 'trapped' in this optical equilibrium position since the optical gradient force is typically on the order of piconewtons (10^{-12} N). It is important to note that, even without the conditions met in the case of stable three-dimensional optical trapping (i.e. tightly focused laser spot), similarly scaled optical forces can be applied by any (less focused or divergent) Gaussian-like laser microbeam.

A particle which is much smaller in size than the incident laser wavelength can be addressed in the Rayleigh regime. This size of particle can be treated as a point electric dipole, which is induced by the external optical (electric) field [30, 31, 32]. As with larger particles which classically reflect and refract incident photons, the electric dipole approximation gives rise to both a scattering and gradient force. The scattering force is due to the absorption and re-radiation of the optical field by the dipole. The gradient forces are due to the inhomogeneous electric field, and are directed along the field gradient. These gradient forces are also proportional the polarizability of the dielectric object. It is important to note that, while the dipole momentum is in fact oscillating in magnitude and direction, the induced dipole momentum remains harmonic with respect to the external optical field. Therefore, the time-averaged gradient force is a non-zero value. The gradient force, to a good approximation, is proportional to the spatial intensity gradient [33].

1.5.2 Single and multi-photon processes in laser-tissue interaction

Ablation is the process of removing material by evaporation, sublimation or plasma formation. Using a pulsed laser with sufficient intensity, light is capable of efficient plasma formation in biological tissues and highly localized ablation. When a laser microbeam is incident upon a biological sample, the sample material absorbs the irradiation either through single photon absorption or nonlinear (multi-photon) absorption,

depending on the irradiation frequency, the intensity (laser power per area) and the pulse duration [34, 35, 36]. While both single photon and nonlinear irradiation can lead to material ablation, single photon absorption can lead to varied deposition of laser energy, causing more extensive damage throughout the cell/sample [34]. It is the peak power of the laser source that dictates the efficiency of the desired nonlinear processes. The peak power, which is defined as $\frac{\text{pulse energy}}{\text{pulse duration}}$, is insufficient to elicit nonlinear absorption in the case of nanosecond pulse durations [35]. It is therefore necessary to shorten the the pulse duration from nanoseconds to femtoseconds (while maintaining constant laser-pulse energy) or increase the laser pulse energy. However, increasing the pulse energy can lead to heating, shockwave production, and cavitation bubble formation, which all lead to spatially extended damage [35, 41,42]. Therefore, nonlinear absorption (and therefore shorter pulse duration) is preferred since it is this multiphoton absorption process that initiates the localized chemical decomposition of the sample [35].

The simultaneous absorption of multiple photons excites a valence electron to a quasi-ionized electron state in the conduction band [28, 35, 36]. This excited electron is the initial 'seed electron' for plasma mediated ablation process. Once the first seed electron has been promoted to the conduction band, it begins to absorb single photons within the pulse duration of the laser, reaching higher energy states within the conduction band [28, 35, 36]. It does this until the kinetic energy of the electron is sufficient to impact ionize a new seed electron from the valence band. Once this happens, these two electrons now repeat the process; reaching the threshold energy necessary to impact-ionize more electrons. Energy is gained by through impact ionization and new seed electrons are promoted to the conduction band until a critical number of these ionized electrons is reached, where decomposition of the material occurs.

$$N_{crit} = \frac{\omega^2 m_e \varepsilon_0}{e^2}$$

Figure 1-2 illustrates the principle of seed-electron recruitment by impact ionization; a total process which is sometimes referred to as cascade or avalanche ionization. For an excitation wavelength of 800nm, N = 10^{21} cm^{-3}. A value at which the plasma becomes reflective [28, 35], and is referred to as the plasma at optical breakdown.

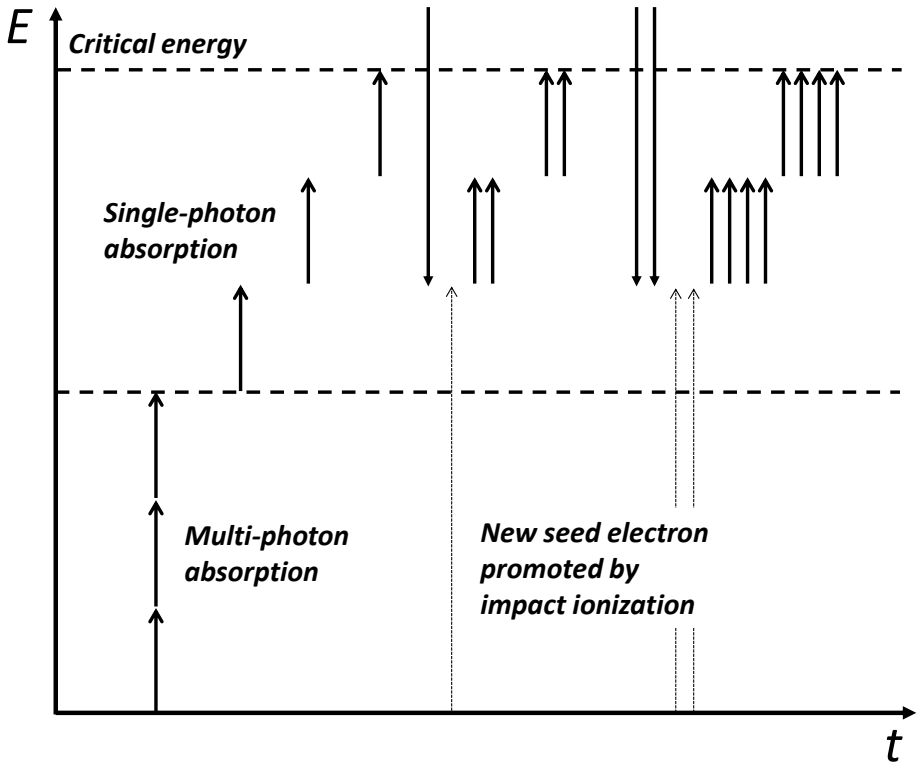

Figure 1:3 Principle of photoionization, impact ionization and free electron avalanche effect (also known as Bremsstrahlung absorption), which leads to plasma formation and tissue ablation.

The combination of the mulitphoton absorption process, the lower threshold energy required for optical breakdown, the lower temperature rise in comparison to

longer pulse durations and the strong confinement of energy in the focal volume are the main factors that make the femtosecond laser an attractive tool for tissue ablation. In addition to the well-defined ablation thresholds associated with femtosecond laser pulses, using NIR wavelengths increases the plasma formation efficiency, since both the plasma absorption coefficient and cascade ionization rate are proportional to the square of the excitation wavelength [28, 35]. Therefore, a shift in the excitation wavelength from the visible (e.g. 532nm) to NIR (e.g. 800nm) increases the production rate of ionized electrons. However, at the expense of shifting the wavelengths to the NIR, a higher pulse energy is required to induce multiphoton absorption. Simulation results have shown that cascade ionization is the more dominant process for creating ionized electrons [35] as opposed to multiphoton absorption alone.

1.6 Closing remarks

A tightly focused fs pulsed laser beam can efficiently ablate biological tissues by plasma mediated process. Laser ablation has proven to be an efficient and reproducible method for performing surgically precise laser induced axotomy for the purposes of studying degenerative and regenerative processes *in vitro* as well as *in vivo*. Estrogen has been implicated in the neuroprotection of CNS axons, which have been shown to have regenerative capabilities. However, the regeneration of mammalian CNS axons is suppressed by environmental factors, including physical barriers which are formed following injury due to natural immunoresponse. Laser microbeams have also been shown to give rise to significant force and temperature gradients in the microscopic regime, while the membranes of neuron growth cones and filopodia contain mechanically and thermally activated ion channels. Ions, especially calcium, have been implicated in axon guidance, as they are integral to polymerization and depolymerization processes which occur inside growth cones and leads to their extension (growth). An influx of

calcium can lead to sustained depolymerization of local filopodia or regions of the growth cone, which are independent from one another. Therefore, we set out to show that a laser microbeam, when placed asymmetrical in the path of an advancing growth cone could effectively guide the growth of an axon in the direction opposite that of the laser beam placement. Furthermore, we wished to study the degeneration and regeneration of primary CNS axons following fs pulsed laser axotomy in the presence and absence of estrogen. Our goal was to begin the development of novel, comprehensive strategies for the treatment of CNS nerve injury, especially those which happen in the spinal cord.

Chapter 2

Evaluation of Regeneration Subsequent to fs Laser Axotomy

2.1 Inroduction

Steroid hormones have significant roles in neurogenesis, neuroprotection and regeneration of injured neurons [37, 38, 39]. They also play critical roles in neuronal structuring in the central nervous system (CNS) [40]. Estrogen induces dendritic spines, creating new synapses in the hypothalamus [43]. Notably, estrogen is well known to have neuroprotective effects.

Laser microbeam provides a unique opportunity to induce highly localized and controlled damage on various parts of the axon, thus allowing study of the relative contribution of localized damage to overall functionality of neuron and subsequent repair process. Using ultrafast laser microbeams [44, 45, 46], whole cells and intracellular organelles can be altered [47, 48] with sub-μm spatial scale with high temporal precision. Laser microbeam can induce such localized damage on the axon without significant damage in more proximal regions. Such microbeams have allowed nanosurgery of individual neuronal axons growing in culture [49] as well as in organisms such as Caenorhabditis elegans [50, 51]. Due to this precision of focused laser beam, combined with non-invasive nature of the near-IR laser microbeam as compared to invasive needles, several measurements on axonal regeneration in PNS have been quantified.

Here, we report impact of estrogen on axonal repair and regeneration subsequent to optic nerve crush as well as laser nanosurgery. Our studies demonstrated that axonal repair and regeneration subsequent to injury made by either classical injury of laser-based axotomy, is stimulated by estrogen (17β-estradiol). Advancement in understanding of the temporal progression and pathophysiology of traumatic axonal injury is imperative for the development of therapies aimed at repairing injured axons and

preventing secondary damage. The ability to study the response of single axons subsequent to highly localized injuries in the presence of protective hormones allows the impactful study of traumatic brain and spinal cord injury *in vitro* as well as *in vivo* [52].

Ultrafast laser axotomy is enabling study of neuronal regeneration in monolayers as well as in 3D environments. Here, we present repair and regeneration of CNS neurons subsequent to distinct degrees of injury associated with varying the intensity and exposure of the incident fs near-infrared laser microbeam. Behavior of regenerated neurons subsequent to laser axotomy and vs detachment resulted in interesting migration patterns and was found to differ. These studies advance our understanding of the spatio-temporal progression of axonal injury and its repair, thus providing a unique opportunity for development of therapies for traumatic brain injuries.

Retinal ganglion cells in fish and amphibians regenerate their axons after transection of the optic nerve [53]. Specialized properties of fish and amphibian visual pathway glial cells and neurons contribute to their successful axonal regeneration. The fish oligodendrocytes lack the axon growth inhibiting molecules that interfere with axonal extension in mammals. Instead, fish optic nerve oligodendrocytes support (*in vitro*) axonal elongation of fish as well as that of rat retinal axons. Moreover, the fish retinal ganglion cells re express upon injury a set of growth associated cell surface molecules and equip the regenerating axons throughout their path and up into their target, the tectum opticum with these molecules. This may indicate that the injured fish ganglion cells reactivate the cellular machinery necessary for axonal regrowth and pathfinding [54].

Understanding axonal pathfinding is key in developing therapies which respond to traumatic CNS or PNS injuries. Laser microbeam^2 provides a unique opportunity to induce highly localized and controlled damage on various parts of the axon, thus allowing

study of the subsequent repair process. However, all the studies have so far been limited to complete dissection of axons (axotomy) [55]. Few recent studies reported repair subsequent to partial axotomy (sub-axotomy) [55, 56, 57]. Though all these studies focused on repair and regeneration kinetics, no clear information about path of regeneration pattern is available so far. *In vivo* nerve repair requires not only the ability to regenerate damaged neurons, but most importantly, the ability of the regenerated axons to find their target guided along the original paths that will result in functional connections. Ultrafast laser axotomy has enabled the study of neuronal regeneration in monolayers as well as in 3D environments. Here, we present repair and regeneration of central nervous system (CNS) neurons subsequent to different types of injury. Behavior of regenerated neurons subsequent to laser axotomy and detachment resulted in interesting migration patterns and was found to differ. These studies advance our understanding of the spatio-temporal progression of axonal injury and its repair; thus providing a unique opportunity for development of traumatic brain injury therapies.

Tightly focused, femtosecond (fs) pulsed laser beams allows the ablation of axonal tissue in highly localized areas for surgically precise axotomy. In this way, axons can be thinned, damaged or severed completely, based on pulse energy, intensity (focus) and exposure. Here, we use these parameters to induce injury of varying severity on Goldfish retinal ganglion axons *in vitro* to show that axonal pathfinding during the regeneration process is dependent on the severity of the injury suffered. These studies advance our understanding of the spatio-temporal progression of axonal injury and its repair, thus provides a unique opportunity for development of therapies for traumatic brain injuries.

Herein, we studied axonal growth rate and regeneration subsequent to laser induced injury in presence and absence of estrogen. Our results shows that growth and

regeneration rate subsequent to retinal explant as well as laser-axotomy are significantly enhanced in retinal ganglion cells of goldfish model.

2.2 Methods

2.2.1 Extraction, preparation, and culture of goldfish retinal ganglion cells

Common goldfish (*Carassius auratus*) retinal ganglion explants were chosen for all degenerative/regenerative studies due to their established ability to regenerate following axotomy [53]. Adult goldfish, 5-7 cm in total body length, were housed in standard glass aquaria at 19°-21°C. In order to facilitate axonal outgrowth in culture, fish received a priming lesion of the optic nerve at least one week prior to removing the retina [58, 59]. Following anesthesia with tricaine methanesulfonate (Argent), the optic nerve was visualized through an incision in the dorsal-posterior conjunctiva and crushed with Dumont #5 forceps in the distal region, where the nerve exits the ocular orbit. Special care was taken to avoid damaging the large blood vessel which runs alongside the optic nerve. One to two weeks after receiving the priming lesion, both eyes were removed from the anesthetized goldfish after following one hour of dark adaptation to facilitate removal of the pigment epithelium, washed in 20% ethanol, and then washed in medium. The retinas were carefully removed, washed twice in medium, and cut into 400 μm square explants on a McIlwain tissue chopper. The explants were then placed into sterile 35 mm Petri dishes with a 14 mm central hole backed with a glass coverslip (MatTek). The coverslip had been previously coated with 0.75 mg/dish poly-D-lysine (Sigma, >300,000 MW in borate buffer, pH 8.3) and 5 μg/dish of laminin (BD Biosciences, in phosphate-buffered saline, pH 7.4). The explants were then oriented by hand so that the ganglion cell side faced towards the laminin, and incubated at room air-mixture and temperature in Leibovitz's L15 medium (Sigma). This medium was supplemented with 10% fetal bovine

serum (Fisher Scientific) and 50 µg/ml gentamicin. Since goldfish are poikilothermic, the retina cells could be imaged *in vitro* at room temperature.

2.2.2 Fs laser axotomy and imaging platform

Figure 2-1 shows the schematic of the microscopic imaging and laser-microbeam manipulation platform. All axon experiments were performed on the same microcope setup with only minor alterations. Fs laser axotomy of healthily advancing goldfish RGC axons was achieved with a tunable Ti: Sapphire laser (MaiTai HP, Newport-SpectraPhysics). Operational pulse width and repetition rate were ~200 fs and 80 MHz (at 785nm) respectively. The beam was operated in mode-lock-on condition to ensure pulsing-mode usage. The near-infrared laser beam was expanded and collimated by 7x beam expander (1 to 7mm) and relayed via folding mirrors (>93% reflectivity) to the back laser port of a Nikon, Ti-U Eclipse inverted microscope. (CL) denotes optional cylindrical lens placement by dashed oval (Figure 2:1), which was used in optical guidance experiments (Chapter 3). The dichroic mirror (DC) and filter set couples the laser beam upwards into the microschope objective (100x,Ph 3, oil immersion, N.A.: 1.3) to form a tightly focuses laser beam, and filters out the downward-path laser beam reflected from the surfaces of the objective and coverslip. This prevents the reflected laser coupling into the oculars or the CCD camera, which can dazzle the field of view. An external mechanical shutter (Uniblitz) was placed in the beam path, and used to activate macropulses of the laser beam. The wavelength and source-power of the laser beam was adjusted via Mai Tai software. Fine adjustments to the sample-site power were made using polarizer (P). Sample site power was calculated by measuring incident beam power below the back aperture of the microscope objective and multiplying this value by the MO transmission coefficient. Since neurons are (semi-) transparent, visualization was achieved using phase contrast microscopy. A phase annulus turret (PAT) was fixed

above the microscope condesnor (C), in the path of the bright field (BF) source, and configured with a phase-3 condenser annulus (to correspond to the microscope objective internal phase plate). Using live image capture, the center of the laser spot was located and marked using ImageJ point tool prior to all experiments. The microscope filter-set was then adjusted to block the reflected laser spot using internal dichroic mirror (DC).

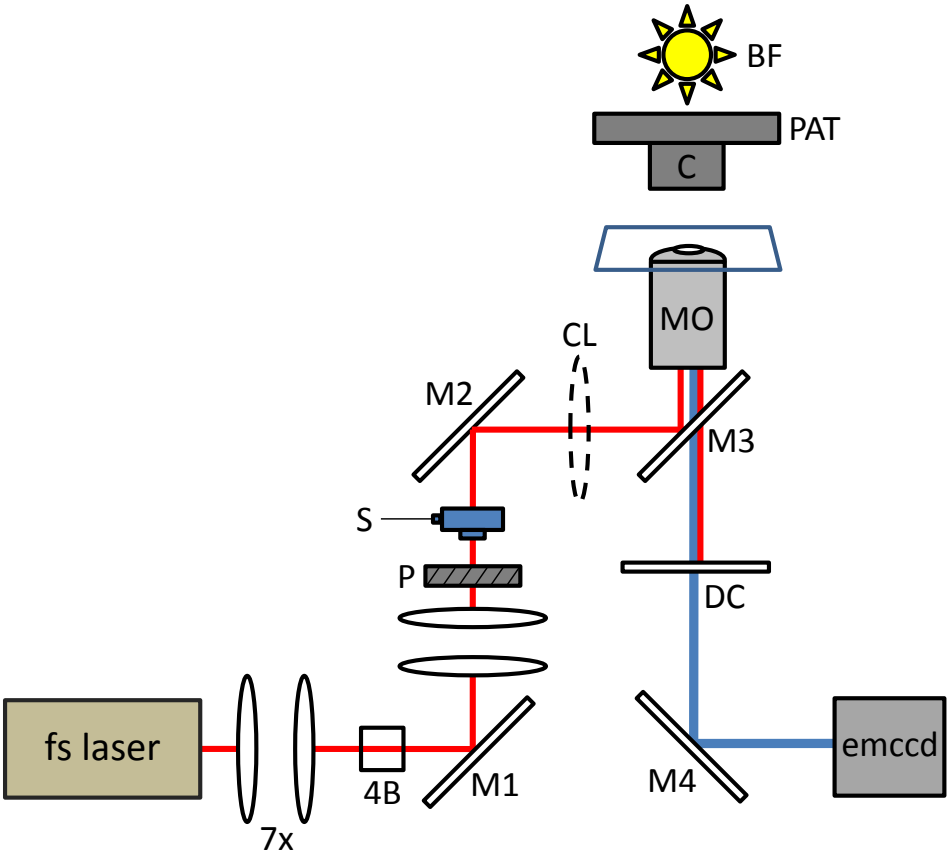

Figure 2:1 Schematic of phase-contrast imaging and laser manipulation platform. fs laser: Femtosecond, tunable TI: sapphire laser. 7x: 7x beam expander and collimator. 4B: Four-way beam splitter. M1, M2: Adjustable mirrors >93% reflectivity. P: Polarizer. S: External controlled shutter (Uniblitz). CL: Replaceable cylindrical lens used to generate

line beam profile. MO: 100x, Phase 3, N.A.: 1.3, oil immersion microscope objective. C: condenser. PAT: Phase annulus turret. BF: Bright field. DC: dichroic. EMCCD: EMCCD camera (Phtotometrics).

2.2.3 Regenerative pathfinding subsequent to varying degrees of initial injury

Fs laser axotomy was performed on 25 healthy, growing RGC axons. Of these axons, 10 (40%) were observed to regenerate within 300 minutes. Axons were injured on the axon shaft, just anterior to the lamellipodium (growth cone) with pulsed sample-site laser power of 150mW (at 785nm). Three distinct and reproducible injuries were performed using varying laser irradiation conditions. For simplicity, I will hereafter refer to these three types of injuries as thin, cut, and burn. Thin injuries (n=4) were achieved by using the external shutter to activate a single 20ms macropulse of fs laser beam (150mW) slightly off-center of the axon's shaft. A cut (n=3) was achieved by activating single 20ms macropule of pulsed laser beam on axial center of the axon's shaft while taking extra care to focus within the transverse diameter of the axon's shaft.

Burn (n=3) injuries were achieved by manually opening (by hand) the external shutter for ~0.25 seconds, with special care taken to center the incident beam on the axial center of the axon, and to focus on the upper plane of the coverslip, where the axon adheres. It is important to note that all reported injuries ultimately resulted is the physical dissociation of the axonal shaft from the lamellipodium (growth cone).

2.3 Results

2.3.1 Regenerative pathfinding subsequent to varying degrees of initial injury

In order to study the effects of varying degrees of initial injury on the degeneration, regeneration, and subsequent pathfinding abilities of primary CNS axons, fs pulsed laser microbeam (785nm) was applied at sufficient power (150mW), focus (1.3 N.A. MO) and repetition rate (80MHz) to effectively ablate tissue on the distal end of axon

shafts in petri dish. Three distinct degrees of initial injury (thin, cut, and burn) were reproducibly applied to randomly selected RGC axons (n=25) by altering the position, intensity (focus) and macropulse exposure of the incident laser beam. Axons which did not regenerate within ~200 minutes following fs laser axotomy were not included in calculations or statistics. Time-lapse images in Figure 2:2 (a) (at t=0 min) show the characteristic differences in the degree of initial injury the axons received. Subsequent time-lapse images (Figure 2:2) illustrate the characteristic differences in degeneration, regeneration, and pathfinding abilities following each type of injury.

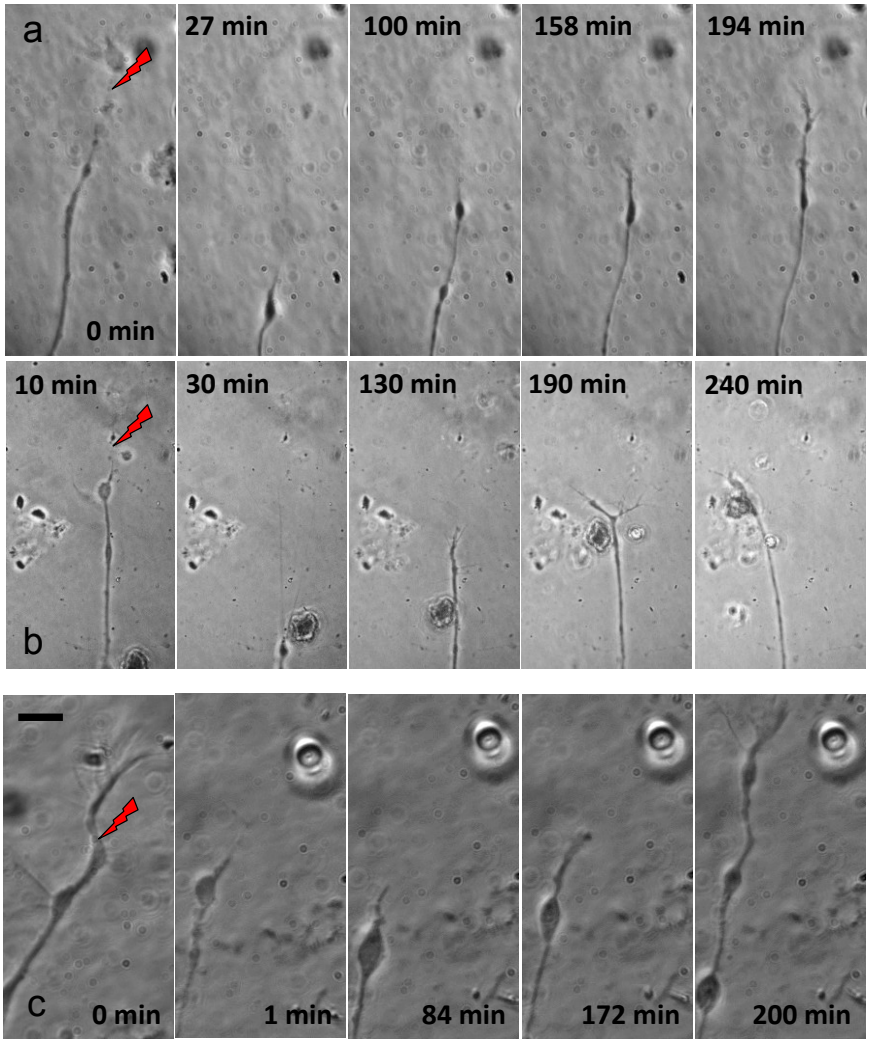

Figure 2:2 Time lapse images of characteristic axonal regeneration and pathfinding ability subsequent to (a) thin, (b) cut, and (c) burn injuries. Fs laser damage sites marked by red lightning bolt. Scale bars represent 6μm.

Degeneration rates were observed to increase with increasing degree of initial injury, while regeneration rates were observed to decrease with increasing degree of initial injury (Figure 2:3). Degeneration rates were 1.15, 0.83, and 3.73 μm/min for thin, cut, and burn injuries respectively. In the case of burn injuries, this increase in degeneration rate may be attributable to the formation of cavitation bubbles (Figure 2:2).

This type of bubble formation may be residue of a shock wave, physically pushing the axon away from the damage site. Furthermore, a shock wave can disburse or destabilize local adhesion proteins and attachment site receptors, such as integrins. Integrins are known to mediate the attachment between axons and the extracellular matrix as well as axonal pathfinding during both developmental and regeneration stages. Integrins have also been implicated in axon fasciculation. The dispersion of these attachment and fasciculation mediating factors would lead to further detachment and disorientation of the damaged axon.

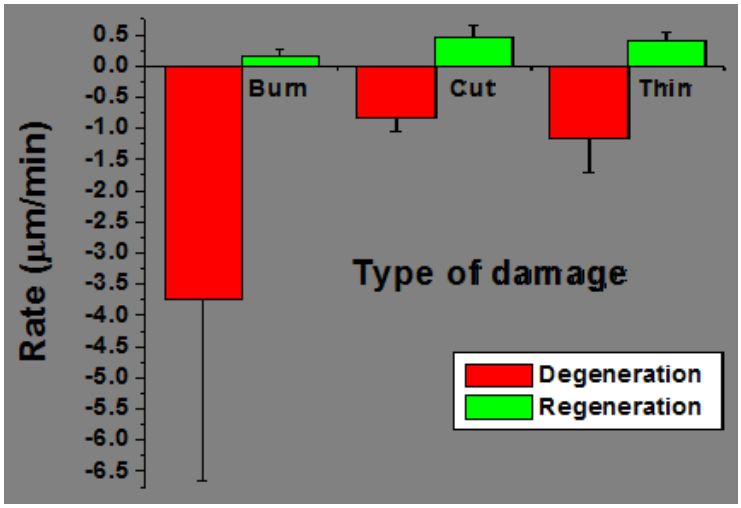

Figure 2:3 Degeneration and regeneration rates of primary RGC axons subsequent to burn, cut, and thin injuries.

Regeneration rates for thin, cut and burn experiments were found to be 0.40 ± 0.14, 0.47 ± 0.17, and 0.16 ± 0.11 µm/min.

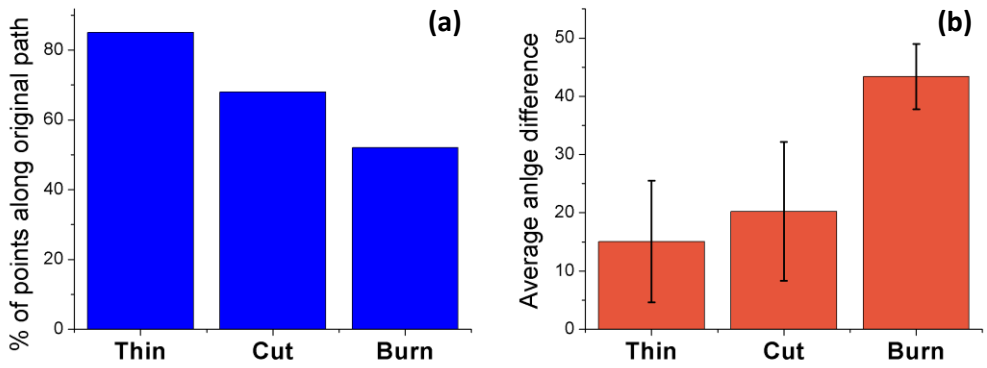

Figure 2:4 (a) Percentage of degeneration and regeneration points found within ±3μm of original path (prior to to injury). (b) Average angle difference between the initial and final orientation of the growth cone (prior to and subsequent to injury) for thin, cut, and burn injuries.

The degeneration and regeneration paths were observed to differ from original outgrowth paths more significantly in the cases of cut and burn injuries, as compared to thinning. This has been quantitatively described in two ways; first, by calculating and comparing the average difference in directional growth cone orientation (relative angle) before injury and at the end of observation (Figure 2:4); secondly, by calculating the percentage of frames (images) in which the leading edge of the growth cone remained within ±3μm of the original outgrowth path during both degeneration and regeneration (Figure 2:4). The average difference in directional growth cone orientation was found to be 15.07 ± 10.44, 20.23 ± 11.91, and 43.41 ± 5.61 degrees for thin, cut, and burn experiments respectively. The percentage of frames in which the leading edge of the axon remained within ±3μm of the original outgrowth path was 85%, 68% and 59% for cut and burn experiments, respectively.

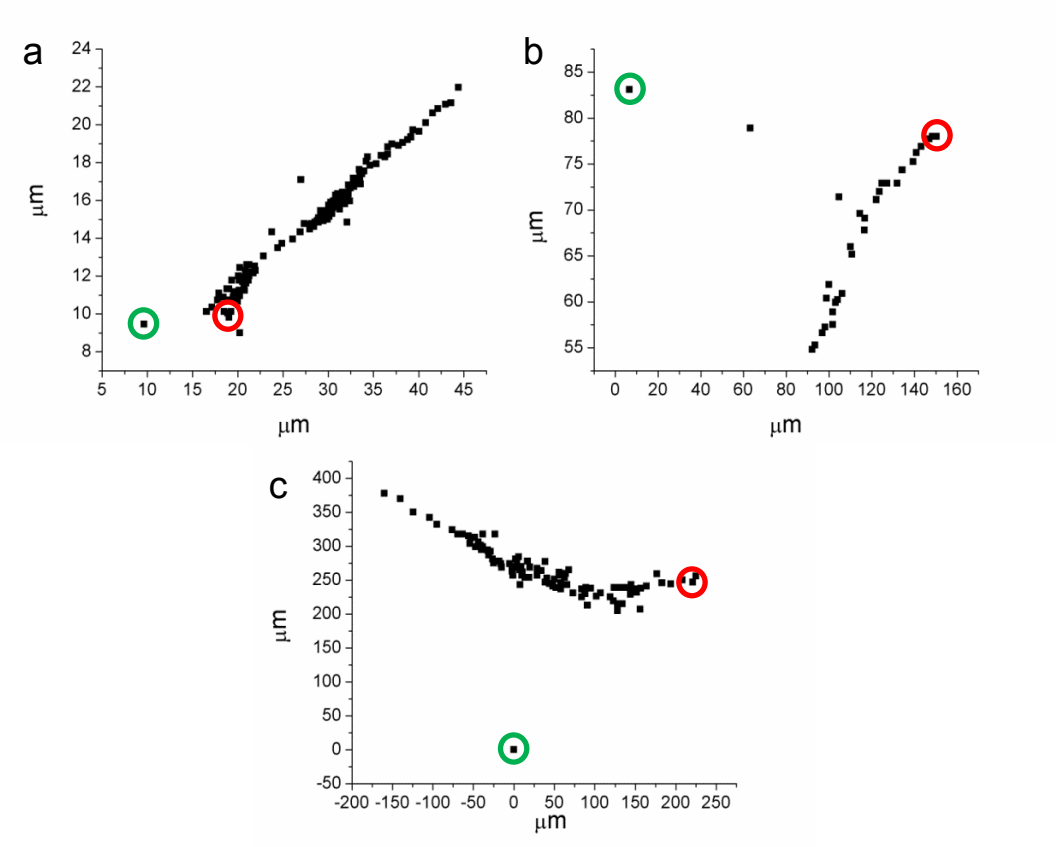

Figure 2:5 Characteristic time plots of leading-edge position of lamellipodia following fs laser induced (a) thin (b) cut, and (c) burn injury. Green circle indicates damage site (initial position) and red circle indicates final position of the lamellipodium's leading edge.

2.3.2 Regeneration in the presence and absence of estrogen

In order to study the role of estrogen in axon repair and regeneration, fs pulsed laser axotomy was performed on RGC axons cultured in the presence of varying concentrations of estrogen (1nM, 10nM, 100nM) as well as control (no estrogen). Axons were injured at the distal end, just before the growth cone, by 20ms macropulse exposure of tightly focused laser microbeam (785nm, 1.3 N.A. MO). This injury was applied to randomly selected axons, whose degeneration and regeneration (in cases which it occurred) was monitored by time-lapse phase-contrast imaging. Figure 2:6 shows

characteristic plots of relative length vs. time for axons following fs laser surgery in the presence of (a) control, (b) 1nM, (c) 10nM, and (d) 100nM concentrations of estrogen.

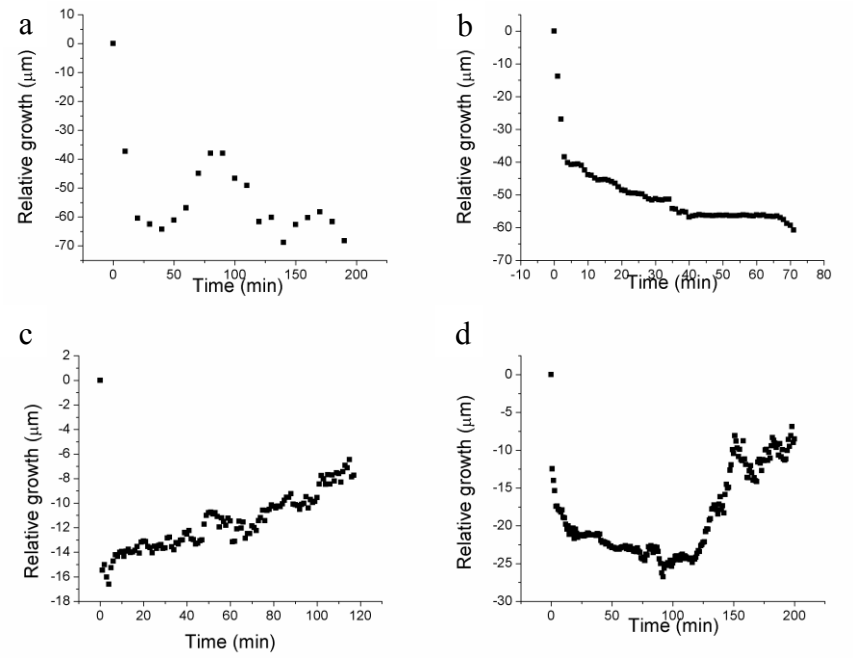

Figure 2:6: Characteristic plots of relative length as function of time for (a) control, (b) 1nM, (c) 10nM, and (d) 100nM concentrations of estrogen

It was observed that estrogen effectively served as a neuroprotective, given the future determination of an optimal concentration for use on RGC axons. FIGURE shows time-lapse images of axon treated with 10nM concentration of estrogen prior (a) and subsequent to (b-d) laser induced axotomy (laser damage spot marked by lightning bolt). The proximal end of the axon is seen to retract immediately following application of fs laser pulse (20ms). Regeneration and repair (observed reformation of growth cone) of the injured axon occurred after only 4 and 60min in cases of 10nM estrogen treatment, whereas no significant growth cone reformation was observed in cases of control axons (imaging up through 270 min). Regeneration occurred in all (100%) experimental

instances involving neurons treated with 10nM estrogen (n=5), whereas control experiments resulted in regeneration in 67% of experiments.

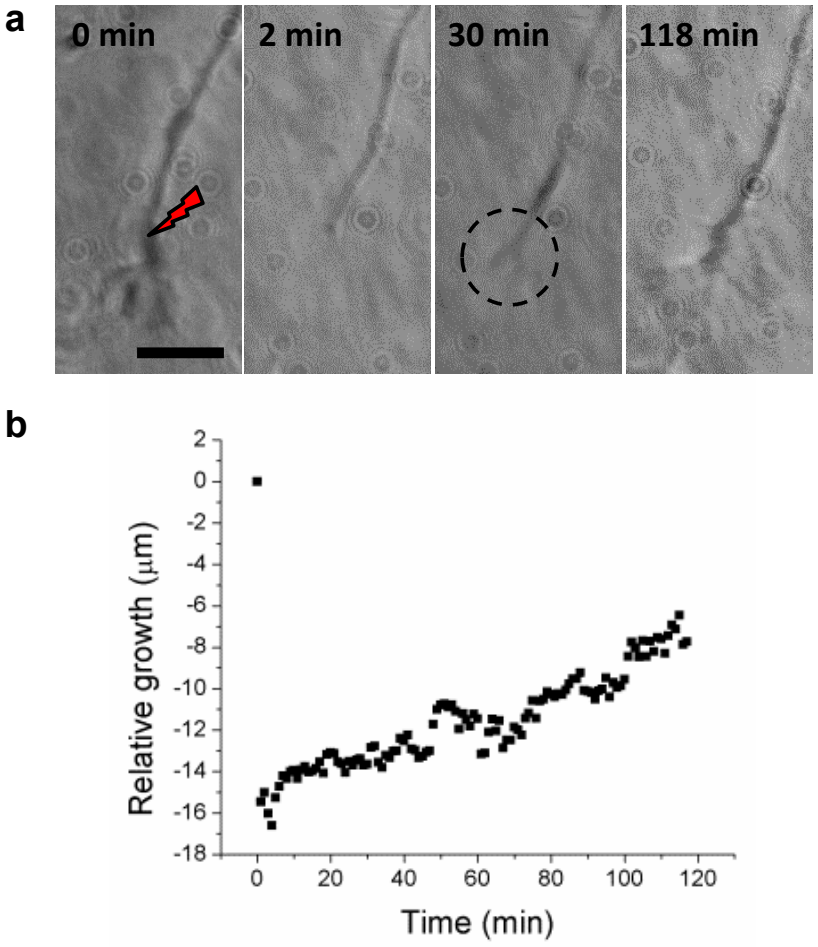

Figure 2:7 (a) Time-lapse images of axon treated with 10nM estrogen prior and subsequent to fs pulsed laser axotomy. Red lightning bolt indicates damage site. Dashed circle highlights observed re-emergence of growth cone. Scale bar represents 6 microns. (b) Corresponding graph of relative length as a function of time following fs pulsed laser axotomy.

Along with likelihood of regeneration, regeneration rates were also found to improve for certain concentrations of estrogen. Regeneration rates following fs laser

injury were 0.23 ± 0.23 μm/min, 0.34 ± 0.22 μm/min, 0.21 ± 0.18 μm/min, and 0.31 ± 0.28 μm/min for 1nM, 10nM, 100nM and control respectively (Figure 2:8c). Furthermore, we observed a statistically significant decrease in the period of time axons treated with 10nM concentration of estrogen degenerated and incubated (Figure 2:8b) as compared to control (no estrogen) (24.25 ± 15.2 min and 0.31 ± 0.28 respectively). There was also an observable decrease in degeneration and incubation period for axons treated with 100nM concentration (31 ± 22.49 min), though it was not statistically significant.

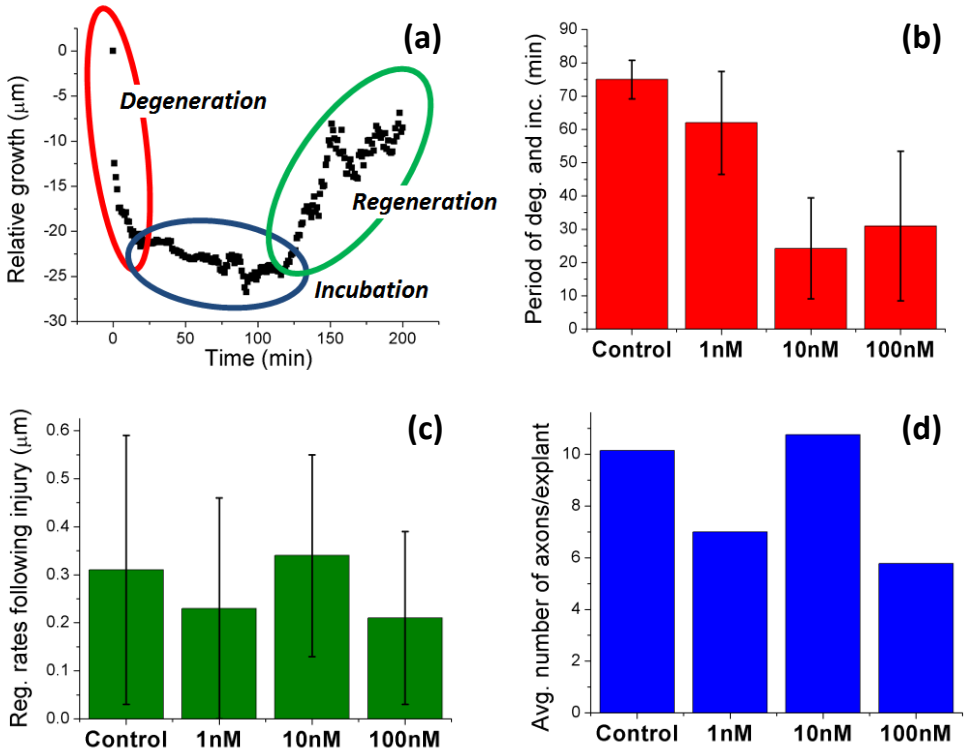

Figure 2:8 (a) What we have defined as degeneration, incubation, and regeneration. (b) Average combined periods of degeneration and incubation following axotomy. (c) Regeneration rates following axotomy. (d) Average number of axons per explant on second day following extraction and culture (9 days following optic nerve crush).

2.4 Conclusions and discussion

2.4.1 Degeneration and regeneration subsequent to various degrees of initial injury

Understanding neuronal regeneration and pathfinding subsequent to injury is the primary step in developing therapies for brain stroke, trauma and spinal cord injuries. We have shown by fs laser axotomy (*in vitro*) that development and regeneration path differences are dependent on the severity of injury in the case of Goldfish retinal ganglion axons. Furthermore, this implies that degenerating axons may leave tracks for themselves to follow subsequent to injury and that these tracks result in a high probability of pathfinding success unless 'derailed' by initial injury or subsequent chemical decomposition of the track.

Axons were shown to degenerate and regenerate different following varying degrees of initial injury. Varying degrees of initial injury produced significant differences in regeneration path as well as axon growth cone orientation (points along original path and angle). Varying degrees of initial injury also produced varying rates of regeneration and degeneration, especially in the case of burn injuries. This may be due to integrin stability during regeneration growth cone pathfinding. Coupling of the cytoskeleton to the substratum is accomplished by specialized receptiors on the surface of the growth cone that recongnize and bind to specific molecules in the outside environment. These recpetors are indirectly linked to the actin cytoskeleton within the growth cone by cross-linking proteins. Receptors that provide this motility-enhancing function include integrins that recongnize extracellular matrix components like laminin, and cadherins. Along with integrins, N-cadherin has been shown to play an important role in axon growth and fasciculation [60]. Cavitation bubble formation may have disbursed these stability and binding factors upon injury. Furthermore, while thin injury ultimately resulted in observed physical dissociation from the lamellipodium, there were initially tubular remnants

observed along the path of degeneration. While the regenerating axon may have used these remnants as a mechanical 'pre-laid track,' it is also possible that chemical factors implicated in fasciculation (i.e. Nogo) may have remained present along with the remnants. Furthermore, cut and burn experiments may have resulted in the spillage of intracellular factors into the medium which could have affected the pathfinding ability of the regenerating axons. The presence and concentration of these factors is, as of yet, unknown and further molecular biology experiments would need to be conducted to implicate or dismiss these factors in pathfinding subsequent to injury.

2.4.2 Regeneration and degeneration in the presence and absence of estrogen

We have confirmed estrogen's neuroprotective qualities as applied to primary RGC axons *in vitro*. However, proving such a role *in vivo* is not straight forward, as animal physiology is not a series of one-step processes. The functions of estrogen are so closely associated with other hormones (androgen, progestin, testosterone), that consideration of estrogen as an independent neuroprotective *in vivo* becomes very difficult [61, 62, 63, 64, 65]. Furthermore, since estrogen is known to stimulate the release of nitric oxide and reduce cholesterol, as well as alter immune functions, the neuroprotective effects of estrogen may be indirect, first altering the health of other organs.

Estrogen also stimulates expression of various neurotrophic factors (e.g. NGF, BDNF) and stimulates axonal regeneration and synaptogensis[66, 67]. However, the detailed mechanism of estrogen mediated neurogenesis, regeneration and repair still remains elusive. Neurotrophins are important regulators of neural development, survival, function, and plasticity [68]. Nerve growth factor (NGF), brain-derived neurotrophic factor (BDNF), neurotrophin-3, and neurotrophin-4, are few well-characterized neurotrophins [68]. Neurotrophin levels are modulated at the sites of injury that affects the neuronal

repair and regeneration processes. Along with neuroptrophins, gonadal hormones such as estrogens and progesterone are also important for neurogenesis and neuroprotection [69, 70, 71].

Chapter 3

Optical Guidance (Light as a Repulsive Guidance Cue)

3.1 Introduction

In vivo nerve repair requires not only the ability to regenerate damaged neurons, but most importantly, the ability to guide developing or regenerating neurons along paths that will result in functional connections. Furthermore, basic studies in neuroscience and neuro-electronic interface design require the ability to construct *in vitro* neural circuitry. Both these applications require the development of a noninvasive, highly effective and efficient tool for axonal growth-cone guidance. Though a myriad of technologies have been introduced based on chemical, electrical, mechanical, optical and hybrid approaches (such as electro-chemical, optofluidic flow and photo-chemical methods), these methods are either less effective or require the introduction of invasive external factors. Here, we demonstrate a novel, purely optical technique that uses low power, near infrared light to guide the growth of common goldfish retinal ganglion cell axons. This non-contact method is highly efficient in realizing large turning angles and is 100% effective.

It is well known that axonal pathfinding [72, 73] is paramount to an organism's nervous system development [74, 75], and that, during this development, functional connections must be made across the entire organism [76, 77, 78] (long range). Further, *in vivo* nerve repair (e.g., following spinal cord injury [79]) requires not only the ability to regenerate damaged axons, but, most importantly, the ability to guide these regenerating axons along paths that will again result in functional connections. Basic studies in neuroscience and design of effective neuro-electronic interface devices [80] require the ability to construct *in vitro* neural circuitry [81]. Therefore, the ability to effectively guide single axons is paramount to the understanding of basic as well as clinical problems. It

has been shown that axonal growth rates and direction, in comparable physiological conditions, are primarily determined by environmental cues [82] which are 'sensed' by the axon's filopodia [72]. These filopodia are finger-like growth cone extensions which sample the surroundings for attractive or repulsive growth cue gradients, which may be mechanical, electrical, or chemical in nature. These cues can effectively induce or inhibit axonal growth [83] by affecting actin filament polymerization processes. If such gradients are asymmetrically positioned along the axonal growth axis, they result in growth cone turning and ultimately short-to-long range axonal guidance (towards or away from the source of the gradient depending on whether it is an attractive or repulsive cue). This has been explained by observations that a growth cone's filopodia react independently to these guidance cues (even independently from the growth cone itself) [72]. For example, activation of a filopodium's calcium ion channels can result in an influx of extracellular calcium, which causes actin depolymerization, resulting in the arrest of filopodium's growth or even complete retraction into the axon's lamellipodium (growth cone) [84]. This has been the basis for several axonal guidance [85] techniques introduced over the past two decades. It has been shown that chemical [86], topographical [87], electrical [88], and hybrid approaches such as electro-chemical [89], optofluidic flow [90] and photo-chemical [91] methods can guide neuronal growth cones *in vitro*. However, these methods are either less effective or invasive, requiring the introduction of external factors. Therefore, the notion of purely optical methods is raising considerable interest.

However, to date, all pure-optical methods (optical tweezers [92], asymmetric line tweezers [93], and ultrafast laser microbeam [94, 95] have been employed as an attractive axonal guidance cue. These methods use a focused laser beam operated in cw or pulsed mode for either optical tweezing (utilizing the intensity gradient) or microsurgery [95] (at the highest intensity region of the beam center). Further, use of these laser micro-

beams as an attractive cue for neuronal growth cone leads to poor guidance ability in terms of efficiency and turning angle of axons. Here, we show that asymmetrical positioning of a laser beam in front of the growth cone produces significant 'axonal growth frustration.' This repulsive optical cue leads to highly efficient and long-range guidance of goldfish retinal ganglion cell axons. Thus, the presented method will allow efficient construction of *in vitro* neural circuitry for study of functional aspects of basic neuroscience and also pave the way for controlling the path of *in vivo* CNS nerve regeneration.

3.2 Material and methods

3.2.1 Optical guidance

Optical guidance experiments on RGC and RCN axons were conducted on the same optical imaging and manipulation platform as discussed in SECTION (Figure 2:1). Phase contrast imaging was used to visualize and capture time-lapse images of RGC and RCN axons. To achieve optical guidance, the center of the laser microbeam was asymmetrically positioned 2-20μm beyond the leading edge of the lamellipodia , in the path of the advancing growth cone. The beam was operated in mode-lock off condition to ensure CW mode usage. The external mechanical (S) shutter (Uniblitz) was used to pulse the laser beam (20 ms ON and 20 ms OFF) in order to avoid mechanical forcing. The wavelength and power of the laser beam was adjusted via Mai Tai laser control software and beam-path polarizer (P) so as to result in a sample-site beam power of ~50 mW for RGC experiments and ~80 mW in the case of RCN experiments. Multi-stage (long range) guidance events were produced by manually repositioning the center of the laser spot to remain in an asymmetric position to induce growth cone guidance. Line beam profiles were generated for use in optical guidance by placing cylindrical lens (CL) in the incident beam path prior to it entering the rear port of the microscope.

3.2.2 Preparation and culture of primary RCN axons

All experimental procedures were conducted according to Institutional Animal Care and Use Committee approved protocol. The cortical neurons were isolated from embryonic 18 day rat embryos (E18). The cortical tissues were dissected, cleaned (meningeal layer), enzymatically dissociated (0.125% trypsin in L-15 medium) for 20 minutes at 37 °C. The dissociated cortical neurons (100,000/device) were seeded on Poly-D-lysine (PDL, 0.01%, Sigma) pre-coated coverglass with Polydimethylsiloxane barrier (Sylgard 184, Dow corning) in serum-free culture medium (Neurobasal medium supplemented B-27 with BDNF and NT-3, 10ng/ml), which was changed every 3 days.

3.3 Results

3.3.1 Optical guidance of goldfish retinal ganglion cell axons

Highly efficient optical guidance of axons using laser as repulsive cue

For optical guidance of axons, *in vitro* experiments were conducted on goldfish retinal ganglion cell axons emerging from retina explants in petridish. Axonal guidance experiments were conducted on the same imaging and manipulation platform as in laser ablation experiments (Figure 2:1). The laser beam (785nm) was asymmetrically positioned in front of randomly-selected, advancing axons in order to turn the growth cone and to ultimately result in axonal guidance. The axons could be selectively turned either “right” or “left,” with turning direction determined by left/right asymmetric placement of the laser spot. Figure 3:1 (a) shows laser spot (average laser power: 50 mW, 25 Hz) being placed to the right forward position of an advancing growth cone. Turning of the axon towards left by more than 40^0 was observed (Figure 3:1 a-b). The axon shaft was found to detach and align itself along this new growth cone direction. This may be attributed to the fact that the flexural rigidity [96] of microtubule (2×10^{-23} Nm^2.)-bundles in axonal-shafts is high enough not to allow sharp turns ($>15^0$). Further, the dynamics of

actin-based motility prefer growth along relaxed, straight paths, as opposed to stressed turns. All sham trials resulted in growth cone passing through phantom laser spot, with negligible (<10°) growth cone turning (n=8). Figure 3:2 shows time-lapse sequence of a sham experiment conducted using phantom laser spot. Axons could also be turned right as effectively as left. Right turn (angle > 30^0) of an axon can be seen (Figure 3:1) as a consequence of left-side placement of laser spot ahead of the advancing growth cone.

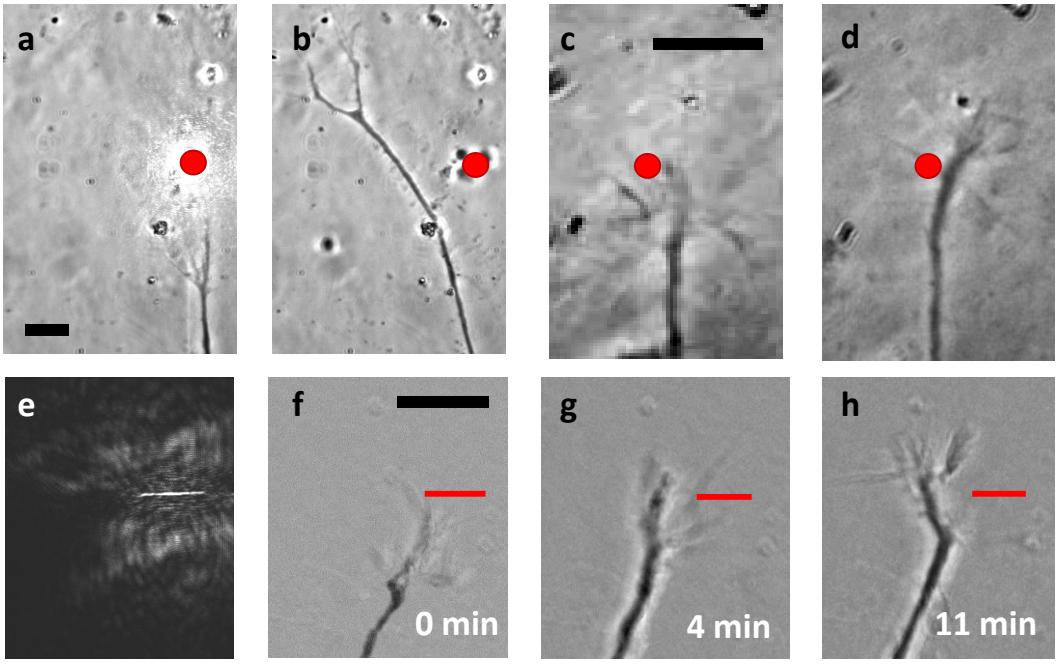

Figure 3:1 Optically controlled axonal guidance, Left-turn before (a) and after (b), Right-turn before (c) and after (d). Spatially-sculpted light for optical guidance: (e) line-spot profile, (f-h) Time-lapse images of axonal guidance using spatially-sculpted line beam profile (marked as red line).

In some cases during single spot-illumination based optical guidance, the leading asymmetric placement did not correlate to oppositely directed guidance due to initial growth cone retraction from the laser spot. Following retraction, the growth cone seemed to “feel out” all new available paths before again interacting with the laser spot,

sometimes generating the unexpected turning direction. However, this effect could be corrected by alternative beam profiles, multiple laser spots, or dynamic control of the laser spot. In order to better define the guidance path, a line beam profile (Figure 3:1 e) was generated by a cylindrical lens, which could be rotated to define the orientation of the profile. Axonal guidance using the line beam profile is shown in Figure 3:1 (f-h), which was achieved using 785nm laser beam. Since the laser power is distributed over a relatively large spatial scale (5μm), higher laser power (200 mW) was used for these experiments. It is worth noting that spatial light modulator (SLM) can be used to define more complex paths for the migrating axons. With time-sharing scanning laser beams, lower power levels can be used to create similar effects.

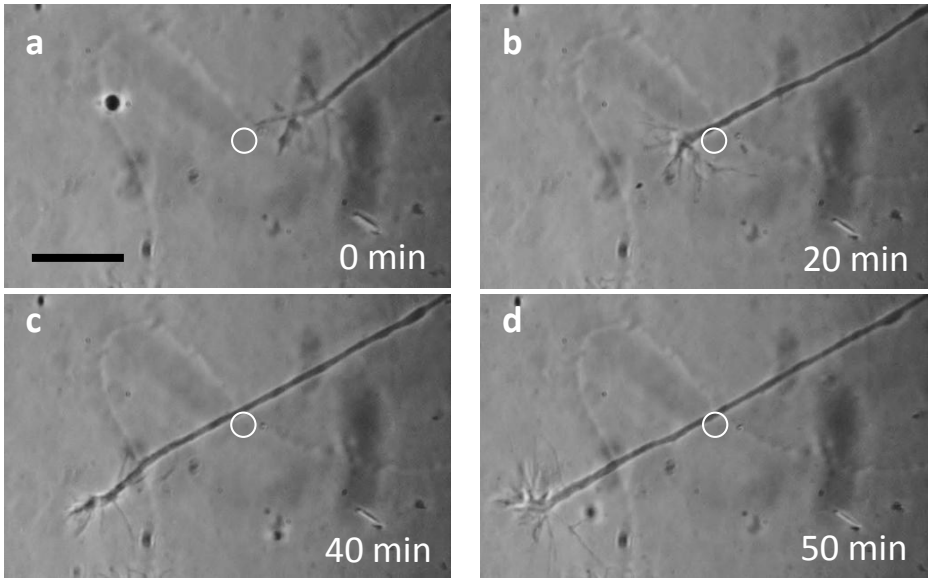

Figure 3:2 Time-lapse images of a sham experiment conducted using phantom laser spot (white circle). Sham experiments resulted in average turning angle of <9 degrees

Kinetics of laser-assisted axonal turning.

For determining the efficacy of optical beam in axonal guidance over a period of time, we tracked a fixed length of axonal shaft (starting from growth cone towards soma)

and overlaid the tracks as illustrated in Figure 3:3 (a). Figure 3:3 (b) shows overlay of time-lapse images of axonal shaft turning towards left due to right-positioning of the laser spot. The kinetics of axonal left-turning angle is shown in Figure 3:3 (c). As shown, the turning process is faster during the initiation phase (5 -10 min), which saturates after 15 min. This behavior is quite similar to that observed during right-turning of axons. In Figure 3:3 (d-e), we show overlay of time-lapse images and kinetics of axonal shaft turning towards right. Figure 3:3 (f) shows cumulative distribution plot for final growth cone turning angles. The majority (8 out of 10) of experiments resulted in growth cone turning angles equal or greater to 42^0, while the remaining (2 out of 10) axons turned $>22^0$ in response to laser spot. Advancing growth cones were turned by an average of 51.1 ± 14.2^0 from their initial paths by single laser spot based optical guidance. Prior to laser spot interaction, the growth rate was 0.73 ± 0.84 μm/min. After the growth cone had turned and was no longer interacting with the laser spot, the observed growth rate became 0.79 ± 0.98 μm/min. Growth Kinetics of a typical axon is shown in Figure 3:4 (d). This clearly indicates that the guidance method is not a permanently damaging event and can be used for guidance and delivery of healthy axons. It is also clear that, while the laser-growth cone interaction is irregular (attraction-repulsion) in nature, the induced repulsive-turn is a permanent event.

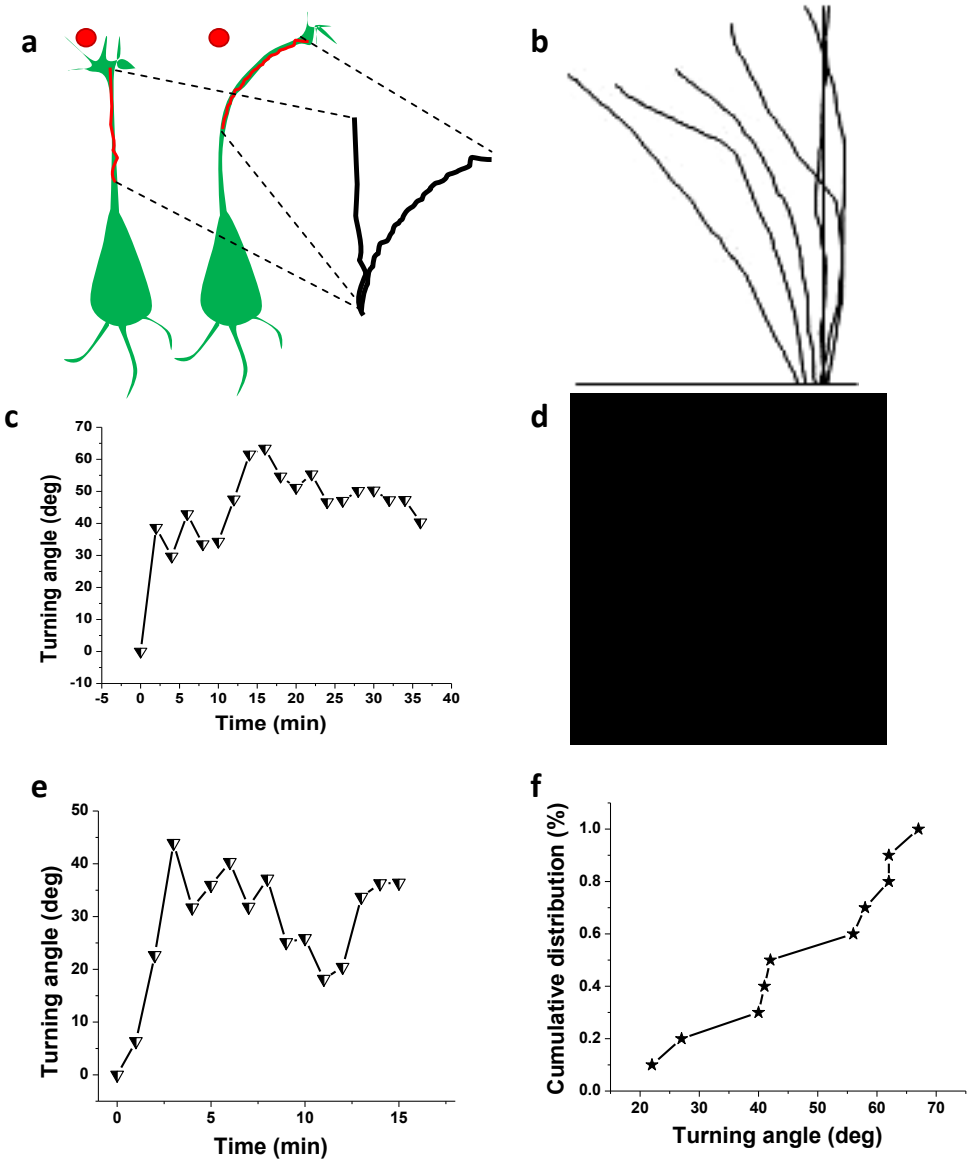

Figure 3:3 (a) Illustration of the method employed for determining efficacy of optical guidance. Laser spot position (red circle). (b) Overlay of time-lapse images of axonal shaft turning towards left. While the axon has advanced during the turning event, along axonal-shaft has been drawn for fixed length. (c) Kinetics of axonal left-turning angle. (d) Overlay of time-lapse images of axonal shaft turning towards right, (e) Kinetics of axonal right-turning. (f) Cumulative distribution plot of initiated turning angles.

Long-range optical guidance of axon.

Long range (both angle and distance) axonal guidance could be realized by effecting multi-staged turns. By relocating the laser spot in front of an already-deviated axonal growth cone path, multi-stage optical guidance was observed to produce an overall turning angle of up to 120 degrees and total guidance distance of ~90μm (Figure 3:4 a-c). After 50min of the start of experiment, the second laser spot was positioned (as shown inFigure 3:4 b) after the axon has turned ~55^0 due to first laser spot (Figure 3:4 a). Figure 3:4 (d) shows kinetics of axonal turning-angle during the multi-stage axonal turning process. The growth rate was found to be low during initial phase (10 min) of interaction with laser spot, which increased after 20 min (once the growth cone has turned completely). Figure 3:4 (e) shows the correlation histogram for growth and turning angle at different time points.

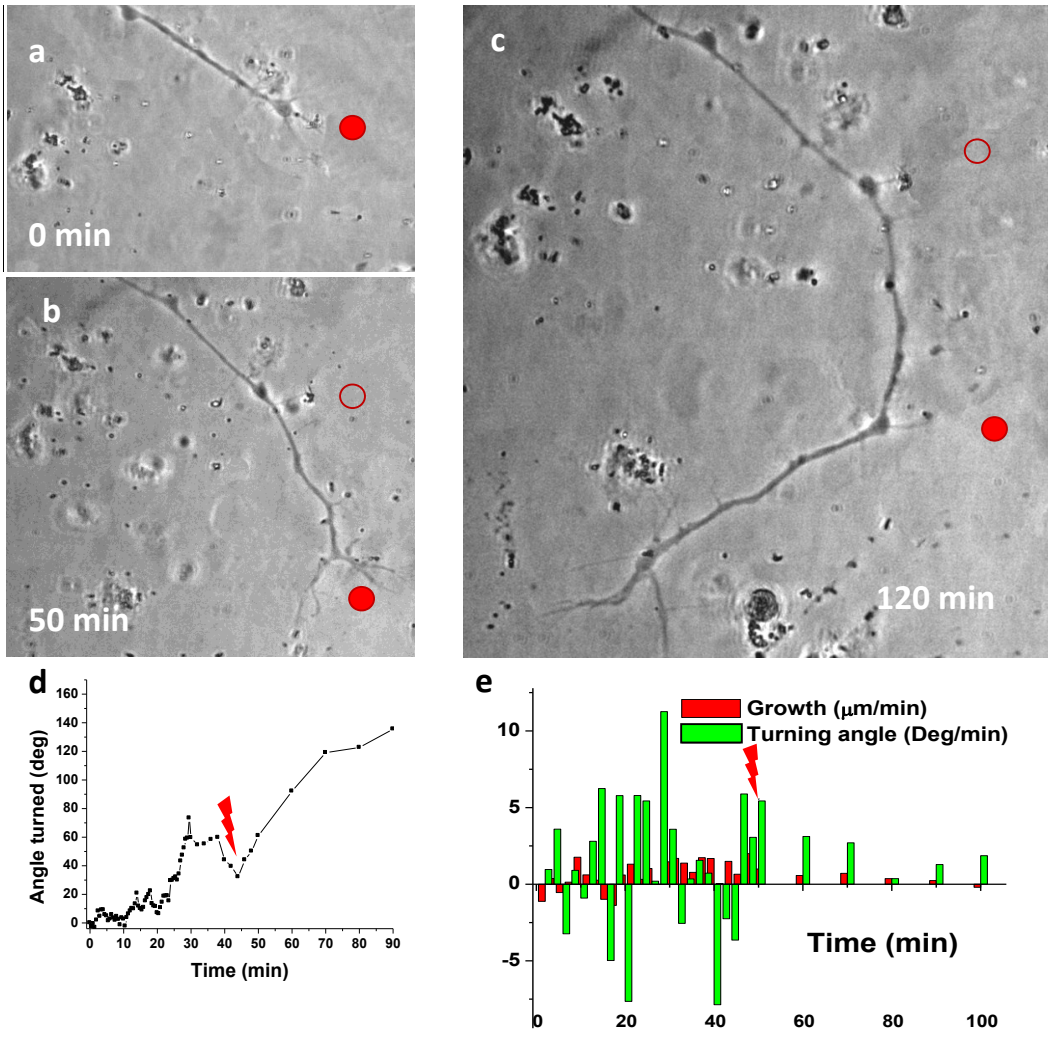

Figure 3:4 (a-c) Time-lapse images of long-range optical guidance using laser spot at multiple sites. The position of laser spot is marked by red filled circles on the images. (d) Kinetics of axonal turning during the multi-stage axonal turning process. (e) Growth and turning angle correlation histogram. The time point of second laser spot irradiation is marked by red arrows in all graphs.

Mechanism of optical repulsive guidance of axon.

The mechanism of repulsive guidance of axon due to laser can be analyzed based on three plausible effects, namely photo-physical, photo-thermal effects (leading to indirect chemical changes) or direct photo-chemical changes during interaction of filopodia with laser spot. Figure 3:5 (a-b) shows time-lapse images of growth cone interaction with laser spot, where the filopodia can be seen to be asymmetrically oriented away from the laser spot. Figure 3:5 (c) shows schematic of filopodia interaction with laser beam, leading to induction of calcium via mechano/thermo-sensitive ion channel (Figure 3:5 d).

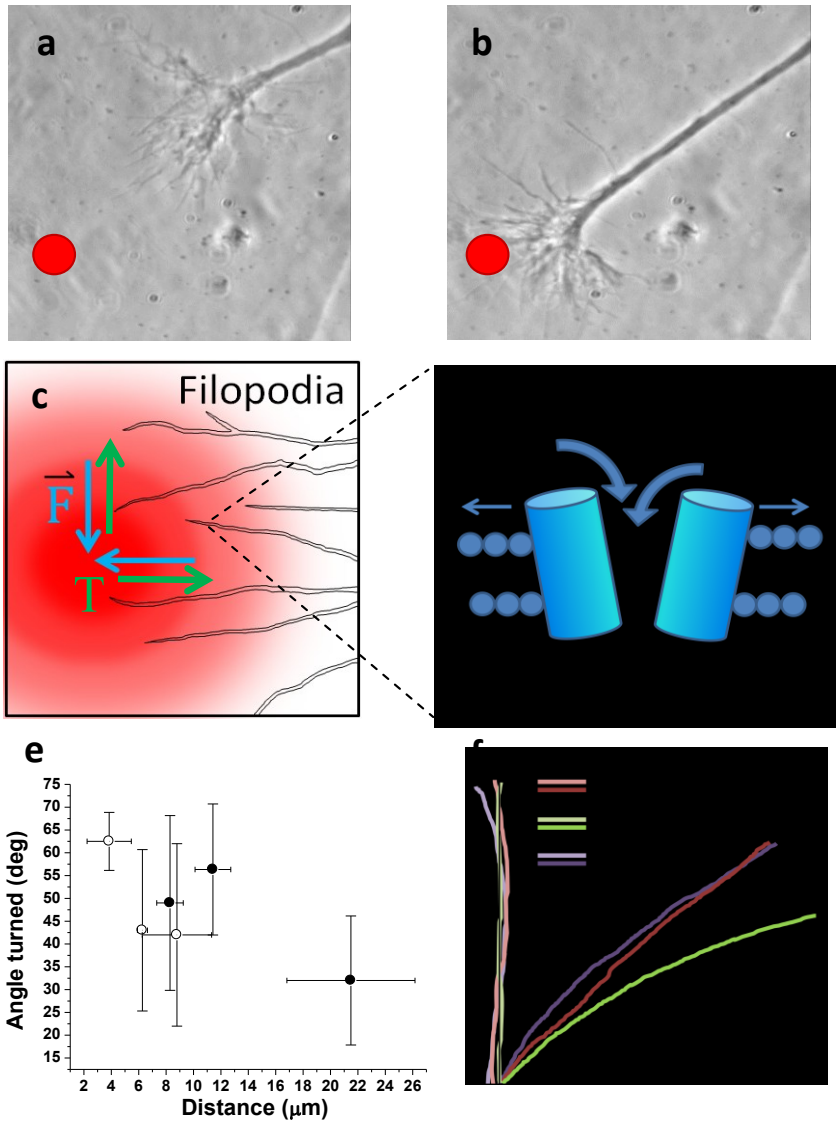

Figure 3:5 (a-b) Time-lapse images of growth cone interaction with laser spot. (c) Schematic of filopodia interaction with laser, (d) Induction of calcium via mechano/thermo-sensitive ion channel in response to laser interaction. (e) Variation of maximum turn angle as a function of initial distance between laser spot and tip of filopodia (open circles) or leading edge of lamellipodia (closed circle). (f) Axonal turning due to laser beam of varying wavelengths. Before turning (faint) and after turning (dark).

To evaluate the effect of radiation pressure force [102] due to laser spot, simulation of both scattering and gradient force on filopodium was carried out. Figure 3:7 shows the estimated forces on the tip of filopodia (diameter: 100 nm, refractive index: 1.4) due to focused laser beam (785 nm) power of 50 mW. While the maximum transverse gradient forces and the axial gradient force are estimated to be in fN range, the scattering force was calculated to be two order of magnitude lower than gradient force. These forces are expected to vary on laser power and on the interaction volume (length) of the filopodium with the laser spot. However, beyond certain threshold (30mW), increase in laser power did not lead to any significant increase in turning angle or efficiency. Further, the axons could be guided with weakly focused (20X, NA=0.5) laser beam, where gradient forces decrease substantially. Therefore, the role of photo-physical forces in the repulsive optical guidance of axons can be neglected.

In order to evaluate role of photothermal effects, axonal turning experiments were conducted at varied distance of laser spot from the filopodium, keeping the laser power fixed. Figure 3:5 (e) shows variation of maximum turning angle as a function of initial distance of filopodium (open circles) from the center of laser spot. Also shown is the turning angle variation with separation of leading edge of lamellopodium (filled circles in Figure 3:5 e) from laser spot. While there is a sharp decrease in turning-angle with increase in filopodium-spot distance, optimal turning angle-distance is still found to be ~3μm away from the laser spot. This action-at-a-distance would indicate involvement of photothermal mechanism and rule out mechanical force or direct photochemical based interaction between laser spot and filopodium. However, since filopodia are highly dynamic, it is possible that filopodia tips may directly interact with laser spot at a height that is not detected during time-lapse imaging. When the laser spot was initially positioned on the filopodium (and/or lamellopodium), the growth cone was found to

retract and terminate (in majority of cases), indicating axonal damage. Therefore, we postulate that filopodium responds to laser-induced thermal gradient leading to the observed repulsive optical guidance.

In order to estimate temperature rise caused by the laser heating of growth medium, simulations were conducted at different wavelengths on the basis of a numerical model (supplementary methods). Figure 3:8 shows the kinetics of estimated temperature rise in the immediate vicinity of the center of the laser spot. Two near-infrared wavelengths (700 and 970 nm) were selected for simulation as absorbance (A) of the medium (water) is quite different at these two wavelengths ($5x10^{-3}$, and $2x10^{-1}$ cm^{-1} for λ=700, and 970 nm respectively). Absorption of the laser energy directly by the filopodium was neglected due to its extremely small thickness and large distance (>2μm, in experimental settings) from the laser spot. Specific heat (*c)* and thermal conductivity *(k)* of water *(*4200 J kg^{-1} K^{-1} and 0.58 W m^{-1} K^{-1} respectively) was used for these simulations. The density of the medium was also assumed same as water, ρ = 1000 kg m^{-3}. As shown in Figure 3:8, the temperature rise in the center of laser spot was found to increase with laser irradiation time. At laser power of 50mW, the saturation temperature rise was estimated to be 0.01, 0.08 and 0.5 K for irradiation wavelengths of 700, 785 and 970 nm respectively. It may be noted that experimentally temperature rise of ~1 K/100mW has been measured [102] at 1064 nm. The saturated estimated peak temperature rise was found to increase linearly with laser beam power. Though temperature rise can affect polymerization of actin directly [103], we believe it is the indirect photothermally driven chemical process which is dominant in our guidance scheme. The spatial distribution of temperature around the center of the focused spot showed that the temperature decreases with increasing distance from the center and levels off at ~2μm from center.

Though the overall temperature rise may seem very low, a temperature gradient of ~ 0.005 to 0.25 K/μm (i.e. 5 to 250 K/mm) is estimated for the laser wavelengths (700-970 nm) and power level (50 mW) used in our experiments. Further, our simulations represent a lower limit of the heating effects, as we have neglected possible higher absorbance of medium relative to that of pure water. It is plausible that growth cone (filopodia) can sense such temperature gradients and guide the axon in response to light beam. For experimental evaluation of the possibility that the turning phenomenon is induced by localized heating effects caused by media's absorption of the laser beam, trials were conducted with λ=700, 785, and 970nm. In spite of the fact that the temperature gradient created by 700 and 970nm laser beams are significantly different, no significant difference in total angle of axonal turning was observed (Figure 3:3 f). This indicates to the possibility that the used power level (50 mW) and associated temperature gradient, even at 700nm, is high enough for inducing repulsion of the growth cone.

It is known that the neuronal growth cone uses surface receptors to integrate the environment and accordingly navigate the axon. Cytoplasmic Ca^{2+} signals have been known [100] to play a key role in this process. The Ca^{2+} regulated motility [104, 105] has been observed to be bimodal in nature, with steep gradients of Ca^{2+} signals mediating attraction and weak gradient of Ca^{2+} signals leading to repulsion. Indeed, earlier studies have shown that lamellipodia extension decreases for laser spots with $\lambda \geq 1200$ nm. This can be attributed to the fact that absorption of water at 1200 nm is an order of magnitude larger than 1064 nm and it is possible that use of 1200 nm heats the medium (and cell) large enough to cause massive membrane depolarization and large Ca^{2+} influx, which can depolymerize the F-actins leading to retraction. In our case, the repulsive nature observed in all laser-growth cone interaction lead us to postulate that the temperature rise due to laser beam leads to gradient of Ca^{2+} signals, which in turn steers the axon

away from laser spot. This constant, local depolymerization leads to a filopodial growth coma in the area of the laser-cell interaction while the rest of the growth cone continues in its polymerization cycle. This directly serves as a guidance cue by retarding local filopodia growth, allowing other filopodia to control the direction of axonal growth. It has been shown [106] that activity of RGCs responds to temperature changes and RGCs are known [107] to express TRPV channels. The TRPV channels are highly sensitive to temperature [108], and essentially serve as cellular membrane “thermometers”. While large temperatures are sensed by activation of TRPV1 & 2 channels, small temperature rise can be detected by TRPV3 and TRPV4 channels. While the mechanism of this optical navigation process will require further investigation, to our knowledge, this is the first successful repulsive optical navigation of axons over large distance and angle. The axonal guidance method reported here can serve as a mean to construct neural circuits.

First, a laser microbeam of Guassian (or similar) cross-sectional intensity profile is known to act as a force gradient, which attracts or pulls objects towards the center of the beam [97]. Stretch-activated (or mechano-sensitive) ion channels are present in virtually all cells [98]. They serve as a primary mechanical transducer, with the channel’s state changing as an immediate effect of mechanical force pressure, or pull [99]. Therefore, any sufficient mechanical force gradient should activate these mechanosensitive channels, resulting in an influx of calcium and other ions present in extracellular media. An influx of extracellular calcium is known [100] to lead to depolymerization of axonal filopodia and, ultimately, the arrestation of the filopodia’s growth (or retraction into the growth cone).

3.3.2 Optical guidance of rat cortical neurons

We successfully extended the optical guidance method detailed in section 3.2.1 to primary rat cortical neuron axons as. 100% efficacy remains while using 80mW

sample-site time-averaged laser power at 785nm wavelength. The average turning angle was found to be 55.3 ± 12.7° (n=4), in excellent agreement with retinal ganglion axon turning angles.

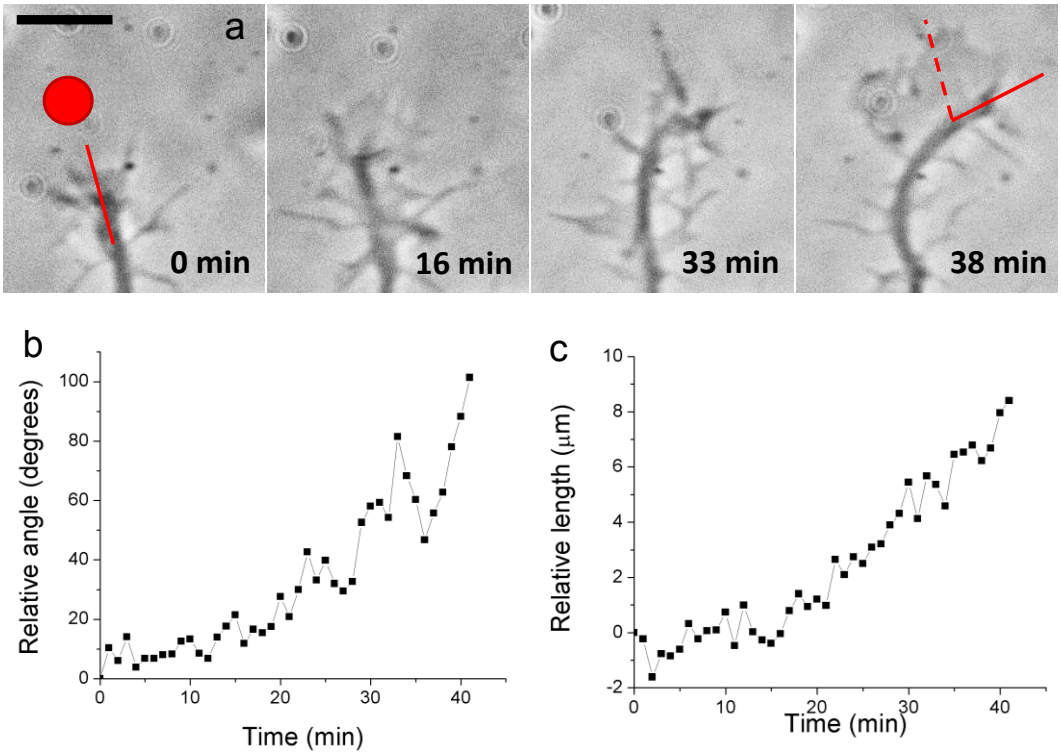

Figure 3:6 (a) Time lapse images showing effective optical guidance of RCN axon. Corresponding relative angle (b) and relative length (c) as functions of time during guidance event.

The wavelength of the optical tweezers needs to be chosen with considerations of possible optical damage and heating. For optical trapping of biological materials, the relative transparent wavelengths are between 750 and 1200 nm (7).

3.3.4 Simulation of force on the filopodia due to laser beam

The gradient trapping force on a spherical Rayleigh object has been derived by Harada et al.[101]. The application of this theory to cylindrical dielectric Rayleigh objects

is a matter of replacing the polarizability constant in the dipole moment equation, as we shall see. Here, we briefly describe the theoretical development of gradient force on a single filopodium (cylindrical, dielectric object assumed to be uniform) as follows. A dielectric filopodium, with radius a, length l, and electric permittivity ε_1 is placed in a medium with an electric permittivity ε_2 and magnetic permeability μ_2, The filopodium is then illuminated by a linearly polarized (electric field taken to be parallel to the X axis) TEM_{00} Gaussian beam, with beam-waist radius $\boldsymbol{W_0}$, which is propagating in the positive Z-direction.

Let the center of the coordinate system (0, 0, 0) be located at the beam waist center and the leading edge of the cylinder be located at $r = (x, y, z)$. Within the zero-order approximation of a paraxial Gaussian beam description, the electric-field vector at the position r is given by $\vec{E}(r) = \hat{x}\vec{E}(r)$ where $\hat{x}$ is the unit vector in the polarization direction. The intensity of light at the position r(x, y, z) can be defined as a time-averaged version of the Poynting vector, and is given by

$$I(r) = \hat{z}\frac{n_2\varepsilon_0 c}{2}|E(r)|^2 = \hat{z}I(r), \tag{1}$$

The intensity profile of a Gaussian (TEM_{00} mode) beam can be written as,

$$I(r) = \left(\frac{2P}{\pi W_0^2}\right)\frac{1}{1+\left(2\tilde{}\right.}\exp(-\frac{2(\tilde{}\quad\tilde{}}{1+(2\tilde{}} \tag{2}$$

in which $P = \pi W_0 n_2 \varepsilon_0 c\frac{E_0^{\ 2}}{4}$, (3)

with E_O being the electric-field strength at the beam-waist center and

$\tilde{}\quad\frac{x}{W_0}$, $\tilde{}\quad\frac{y}{W_0}$ and $\tilde{}\quad\frac{z}{\pi W_0\tilde{}}$. (4)

The filopodium (radius: a, length: l) in the instantaneous electric field of $\vec{E}(r,t)$ acts as a simple cylindrical dipole, located at its center, whose dipole moment in MKS units is given by

$$\boldsymbol{p}(\boldsymbol{r},t) = 2\pi n_2^2 \varepsilon_0 a^2 l \left(\frac{m^2-1}{m^2+1}\right) \boldsymbol{E}(\boldsymbol{r},t) \quad (5)$$

where m = n_1/n_2 is the relative refractive index of the filopodium, and $2\pi n_2^2 \varepsilon_0 a^2 l \left(\frac{m^2-1}{m^2+1}\right)$ is the polarizability of right circular cylinder, assuming that the orientation of the electric field is perpendicular to the axial direction of the cylinder [109]. There are no closed-form solutions for a dielectric right circular cylinder without this assumption, and the problem must be solved numerically since circular cylinders are objects with uniaxially anisotropic polarizability. Even then, the polarizability is often calculated for a spheroid since closed-form solutions exist [110].

The gradient force is due to the Lorentz force acting on the dipole induced by the electromagnetic field. By using the electric dipole moment, an instantaneous gradient force can be described as

$$\boldsymbol{F}_{grad}(\boldsymbol{r},t) = [\boldsymbol{p}(\boldsymbol{r},t)\cdot\boldsymbol{\nabla}]\boldsymbol{E}(\boldsymbol{r},t) \quad (6)$$

$$= 2\pi n_2^2 \varepsilon_0 a^2 l \left(\frac{m^2-1}{m^2+2}\right) \frac{1}{2} \boldsymbol{\nabla} \langle \boldsymbol{E}^2(\boldsymbol{r},t) \rangle_T \quad (7)$$

$$= \frac{\pi n_2^2 \varepsilon_0 a^2 l}{2} \left(\frac{m^2-1}{m^2+2}\right) \nabla |E(r)|^2 \quad (8)$$

where the vector identity of $\nabla \vec{E}^2 = 2\left(\vec{E}.\nabla\right)\vec{E} + 2\vec{E}x\left(\nabla x\vec{E}\right)$ has been used with $\nabla x\vec{E} = 0$, as a result of the Maxwell's equations. The gradient force which the filopodium experiences in a steady state is the time-average version and is given by

$$= \frac{\pi n_2 a^2 l}{c} \left(\frac{m^2-1}{m^2+2}\right) \nabla I(r) \quad (9)$$

By substitution, the x and z components of the gradient force are:

$$F_{grad,x}(r) = -\hat{x}\frac{\pi n_2 a^2 l}{c}\left(\frac{m^2-1}{m^2+2}\right)\left(\frac{4\hat{x}/W_0}{1+(2\hat{z})^2}\right)I(r) \quad (10)$$

$$F_{grad,z}(r) = -\hat{z}\frac{\pi n_2 a^2 l}{c}\left(\frac{m^2-1}{m^2+2}\right)\left(\frac{8\hat{z}/(kW_0^2)}{1+(2\hat{z})^2}\right)\left(1-\frac{2(\hat{x}^2+\hat{y}^2)}{1+(2\hat{z})^2}\right)I(r) \quad (11)$$

Figure 3:7 shows simulations of optical gradient forces acting on a dielectric cylinder at varying laser wavelength and average laser powers.

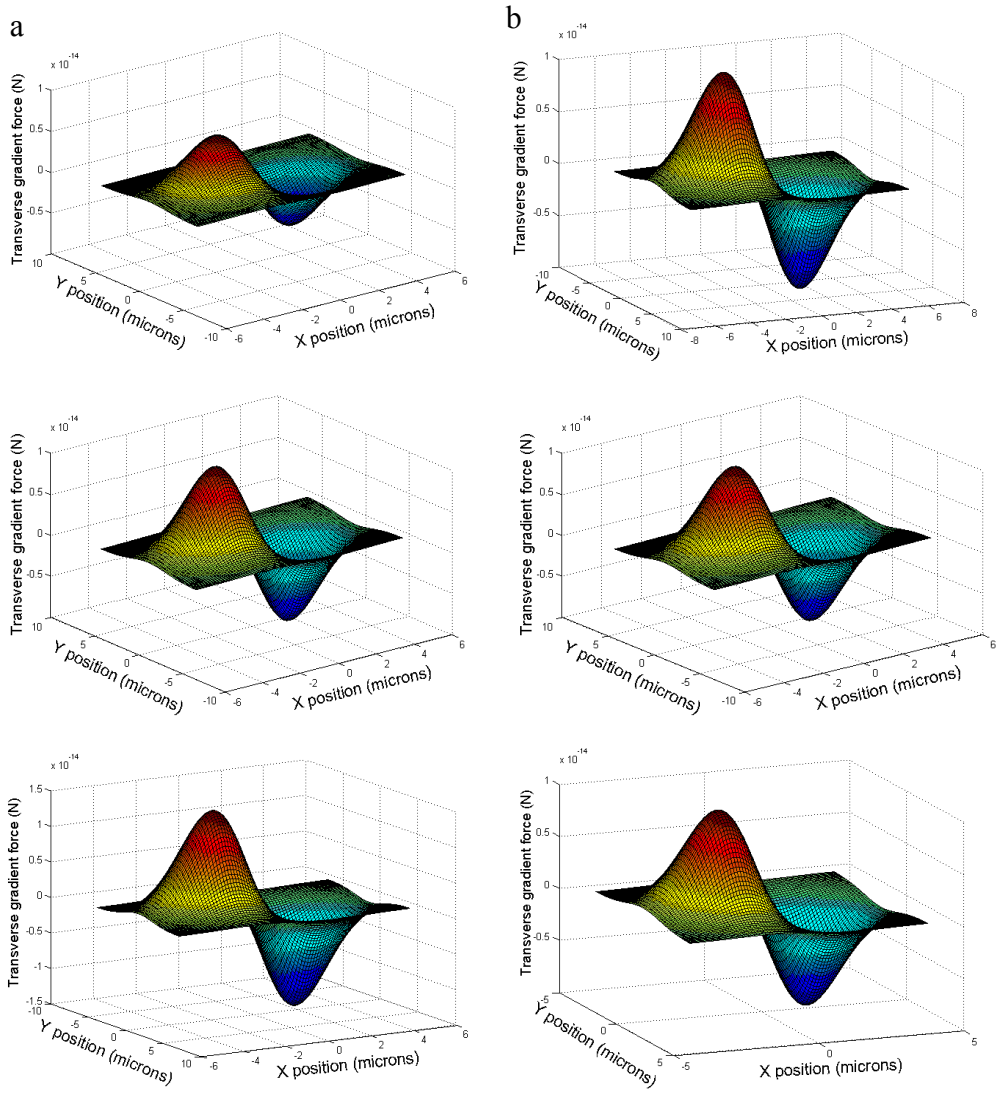

Figure 3:7 (column a) Simulation of optical force acting on dielectric cylinder (diameter: 100nm, refractive index: 1.4) due to focused laser beam with fixed wavelength (785nm) and varying laser power (50, 80, 100mW). (column b) Simulation of optical transverse gradient force acting on dielectric cylinder with fixed power (80mW) and varying wavelength (690, 785, and 900nm).

3.3.5 Theoretical calculation of the local temperature rise by laser

The local temperature rise as a result of the laser heating of growth medium at different wavelengths was calculated on the basis of a numerical model. The laser-heated medium was assumed to be the only point sources of heat. Evaporation of water as a cooling mechanism was neglected. The temperature rise of medium was estimated by considering two concurrent processes: heat generation in the medium by absorption of the laser beam and heat depletion into the surrounding media by the process of conduction. Accordingly, these two processes were modeled in spherically symmetric coordinates into the Fourier heat equation,

$$\rho c(\frac{\partial T}{\partial t}) = \frac{k}{r^2}\frac{\partial}{\partial r}(r^2\frac{\partial T}{\partial r}) + Q_s \qquad (12)$$

where T is the temperature (K), ρ is the density (kg /m^3), c is the specific heat capacity of the medium (J kg^{-1} K^{-1}), k is the thermal conductivity of the medium (W m^{-1} K^{-1}), t is the time (s), Q_s is the heat-source term (W/m^3) due to the heating by the continuous wave laser excitation and r is the radial distance (m) from the focused spot. Assuming that 100% of the energy absorbed by the medium is transferred to the surroundings as heat, Using Beer–Lambert's law: $A = -\log(1-Q_s/Q) = \varepsilon c l$, where A: absorbance of the medium. Q is the incident laser power per unit volume (W/m^3) in the focal spot, ε: extinction coefficient, l: path length), Q_s becomes equal to the laser power absorbed by the medium per unit volume;

$$Q_s = Q(1-10^{-A}) \qquad (13)$$

The heating control volume (m^3) for the calculation was based on the radius of focal spot (R= 0.4μm) and path length l (depth of focus= $2\pi R^2/\lambda$) of 1μm. The heat transport equation was solved by an explicit finite-difference method given by

$$\rho c\left(\frac{T_{i+1j}-T_{ij}}{\Delta t}\right)=k\left(\frac{T_{ij-1}-2T_{ij}+T_{ij+1}}{(\Delta r)^2}\right)+Q_s \tag{14}$$

where *Δt* and *Δr* are the characteristic time and distance steps, and *i* and *j* are the corresponding indices. A stability criterion[40] for the finite difference method is given by

$$\Delta t \le \frac{2\rho c(\Delta r)^2}{k} \tag{15}$$

thus imposing a constraint on the value of *Δt* for a selected value of *Δr.* A decrease in *Δr* affords a higher accuracy, but at the expense of a quadratic increase in the number of time-step computations. The distance step *Δr* was selected to be 100 nm whereas *Δt* was evaluated (to be 145 ns) from the limiting condition of the stability criterion.

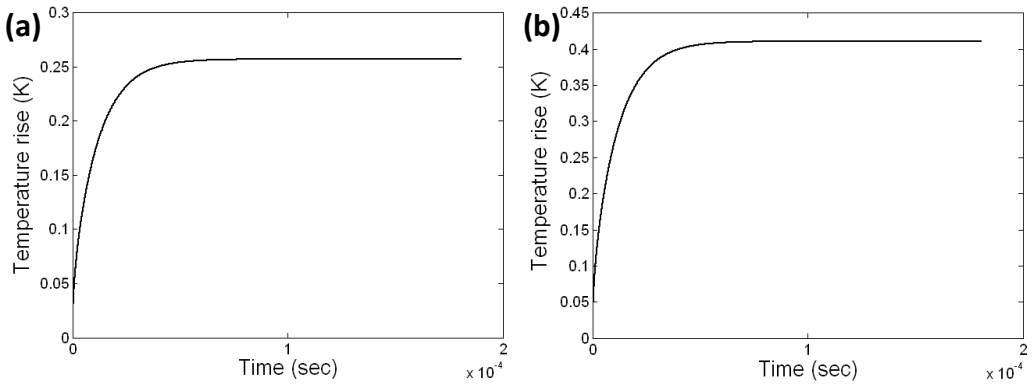

Figure 3:8 Estimate and dynamics of calculated temperature rise for focused laser beam of fixed wavelength (785nm) at (a) 50mW and (b) 80mW.

3.4 Discussion

3.5 Closing remarks

We have demonstrated a novel laser-based method for the efficient guidance of neurons which does not require optical tweezers or microfluidic flow. This method was successful for both permanent short and long range axonal guidance, as we observed

guidance of not only the lamellipodial extension, but of the axonal shaft as well. This non-contact method permits multiple and sequential operations to be performed on a single growth cone. We have also demonstrated that both laser spot and spatially-sculpted line beam results in significant growth cone turning, independent of operational wavelength. The optimization of effective laser profiles, as well as the integration of automated laser/stage systems should allow for dynamical control of axonal growth paths. Further, by using high speed spatial light modulator and several laser beams, it should be possible to create multiple, spatially-sculpted light spots in order to allow simultaneous control of one or more growth cones.

Although the mechanism (or combination of mechanisms) at work here require further elucidation, we believe that activation of stretch-activated ion channels can be tentatively ruled out. Stretch-activated ion channels have been shown capable of activation following application of 40mmHg reverse pressure. This reverse pressure, when being applied directly along the axial direction of a single filopodia, would require an optical force on the order of 10^-9N. According to our force simulations, the optical force acting on a single filopodia is on the order of 10^-14N. Furthermore, the directional range at which this gradient force is attractive is approximately ±2μm from the center of the laser spot. Outside this range, the gradient force is repulsive. However, we have shown successful guidance with laser spot initially positioned more than 10μm away from the growth cone. This does not mean that the guidance event began at this point, but that the growth cone advanced towards and into the force gradient, which would have been repulsive at displacements greater than ~2μm. It should be noted, however, that in some circumstances, changing the relative concentrations of calcium ions within the growth cone can switch the effect of several guidance cues from attraction to repulsion or vice versa.

It is also important to note that, whether the mechanism responsible for repulsive optical guidance is shown to be photomechanical, photothermal, or photochemical, the mechanism does not rely exclusively on a tightly focused laser beam (i.e. optical tweezers), and should therefore be realizable using fiber optics. As a fiber optic technique, this method of axonal guidance has potential for future clinical research and applications.

Chapter 4

Conclusions and Future Directions

Future advancements in the prevention and treatment of traumatic axonal injury will be predicated on our collective understanding of the relationship between the biomechanics and pathophysiology of various phases of axonal damage. Here, we have demonstrated the effects of varying degrees of injury on primary RGC axons, as well as the role of estrogen as a neuroprotective. Furthermore, we have demonstrated a novel, non-invasive technique for the optical guidance of primary RGC as well as RCN axons *in vitro*. The combined of these experiments have elucidated a potential program for the treatment of catastrophic axonal injury *in vivo*. We are currently developing an *in vivo* spinal cord model and demonstrating guided fasciculation of rat cortical neuron axons onto dorsal root ganglion axons in the antiparallel direction in channels which simulate the interior of the spinal cord.

Future experiments will be geared towards the determination of guidance mechanisms and optimization of *in vitro* RCN guidance. The determination of guidance mechanisms will likely be determined through a combination of calcium, antibody, and mitochondrial staining. If it is shown that temperature gradients are responsible for optical guidance, our results would potentially improve by shifting the guidance wavelength further into the infrared, since the interaction (possible damage) between the laser and axon would decrease while the temperature gradient (media absorption) would increase. Furthermore, it will be extremely important to successfully demonstrate repulsive optical guidance using defocused light. To do so would be to demonstrate the possible extension of this method to fiber optics. In addition to fiber optics, we plan to use spatial light modulators (SLMs) to construct an effective laser net, or grid, through

which axons could be guided. In this way, we could study neural circuitry and construct simple neural computers.

References

1 Pugh, G.E. The Biological Origin of Human Values, New York, Basic Books1977.

2 Davenport, R.W., Dou, P. Mills, L.R., Kater, S.B., J. Neurobiology, Distinct calcium signaling within neuronal growth cones and filopodia, 1996m Sep, 31(1); 1-15.

3 Hutson, L.D., Chien, C.B., (2002) Pathfinding and error correction by retinal axons: the role or astray/robo2. Neuron 33: 205-217

4 Kakulas, B.A. (1999) A review of the neuropathology of human spinal cord injury with emphasis on special features. J. Spinal Cord Med. 22:119-124.

5 Cajal, SRy (1928) Degeneration and regeneration of the nervous system. London: Oxford Univ. Press.

6 Aguayo, A.J., David, S., Bray, G.M. (1981) Influences of the glial environment on the elongation of axons after injury: transplantation studies in adult rodents. J. Exp. Biol. 95: 231-240.

7 Goodman, J.H., Bingham, W.G., Jr., Hunt, W.E. (1979) Platelet aggregation in experimental spinal cord injury. Ultrastructural observations. Arch. Neurol. 36: 197-201.

8 Wallace, M.C., Tator, C.H., Frazee, P. (1986) Relationship between posttraumatic ischemia and hemorrhage in the injured rat spinal cord as shown by colloidal carbon angiography. Neurosurgery 18: 433-439.

9 Shi, R., Pryor, J.D., (2002) Pathological changes of isolated spinal cord axons in response to mechanical stretch. Neuroscience 110: 765-777.

10 Hagg, T., Oudega, M. (2006) Degenerative and spontaneous regenerative processes after spinal cord injury. J. Neurotrauma 23: 264-280.

11 Jones TB, McDaniel EE, Popovich PG (2005) Inflammatory-mediated injury and repair in the traumatically injured spinal cord. Curr Pharm Des 11:1223-1236.

12 Tator CH, Fehlings MG (1991) Review of the secondary injury theory of acute spinal cord trauma with emphasis on vascular mechanisms. J Neurosurg 75:15-26.

13 Kreutzberg GW (1996) Microglia: a sensor for pathological events in the CNS. Trends Neurosci 19:312-318.

14 Schnell L, Schwab ME (1990) Axonal regeneration in the rat spinal cord produced by an antibody against myelin-associated neurite growth inhibitors. Nature 343:269-272.

15 Silver J, Miller JH (2004) Regeneration beyond the glial scar. Nat Rev Neurosci 5:146-156.

16 Reier P (1986) Gliosis following CNS injury: the anatomy of astrocytic scars and their influence on axonal elongation. New York: Academic Press.

17 Hall ED, Pazara KE, Linseman KL. Sex differences in postischemic neuronal necrosis in gerbils. J Cereb Blood Flow Metab 1991;11:292–298. [PubMed: 1997500]

18 Roof RL, Hall ED. Estrogen-related gender difference in survival rate and cortical blood flow after impact-acceleration head injury in rats. J Neurotrauma 2000;17:1159–1169

19 Murphy SJ, McCullough LD, Smith JM. Stroke in the female: role of biological sex and estrogen. ILAR J 2004;45:147–159. [PubMed: 15111734]

20 Roquer J, Campello AR, Gomis M. Sex differences in first-ever acute stroke. Stroke 2003;34:1581–1585. [PubMed: 12805490]

21 Niewada M, Kobayashi A, Sandercock PA, Kaminski B, Czlonkowska A. Influence of gender on baseline features and clinical outcomes among 17,370 patients with confirmed ischemic stroke in the international stroke trial. Neuroepidemiology 2005;24:123–128. [PubMed: 15637449]

22 Wilson ME, Liu Y, Wise PM. Estrogen enhances Akt activation in cortical explant cultures following neuronal injury. Brain Res Mol Brain Res 2002;102:48–54. [PubMed: 12191493]

23 Wilson ME, Dubal DB, Wise PM. Estrogen protects against injury induced cell death in cortical explant cultures: a role for estrogen receptors. Brain Res 2000;873:235–242. [PubMed: 10930549]

24 Sortino MA, Chisari M, Merlo S, Vancheri C, Caruso M, Nicoletti F, Canonico PL, Copani A. Glia mediates the neuroprotective action of estrogen on beta-amyloid-induced neuronal death. Endocrinology 2004;145:5080–5086. [PubMed: 15308615]

25 Tripanichkul W, Sripanichkulchai K, Finkelstein DI. Estrogen down-regulates glial activation in male mice following 1-methyl-4-phenyl-1,2,3,6-tetrahydropyridine intoxication. Brain Res 2006;1084:28–37. [PubMed: 16564034]

26 Morale MC, et al. Estrogen, neuroinflammation and neuroprotection in Parkinson's disease: glia dictates resistance versus vulnerability to neurodegneration. Neuroscience 2006;138:869–878. [PubMed: 16337092]

27 Oraevsky AA, Silva LBD, Rubenchik AM, Feit MD, Glinsky ME, Perry MD, Mammini BM, Small W, Stuart BC: Plasma Mediated Ablation of Biological Tissues with Nanosecond-to-Femtosecond Laser Pulses: Relative Role of Linear and Nonlinear Absorption. IEEE J Quantum Elect 1996, 2(4): 801-809.

28 Niemz M: Laser-Tissue Interactions: Fundamentals and Applications, Second edn: Springer-Verlag Berlin Heidelberg New York; 2002.

29 A. Ashkin, “History of optical trapping and manipulation of small-neutral particle, atoms, and molecules,” *IEEE Journal of Selected Topics in Quantum Electronics*, Vol. 6, No. 6, pp. 841-859, 2000.

30 K. C. Neuman and S. M. Block, “Optical trapping,” *Review of Scientific Instruments*, Vol. 75, No. 9, pp. 2787-2809, 2004.

31 D. Mcgloin, “Optical tweezers: 20 years on,” *Philosophical Transactions of the Royal Society A-Mathematical Physical and Engineering Sciences*, Vol. 364, pp. 3521-3537, 2006.

32 M. M. Burns, J. Fournier and J. A. Golovchenko, “Optical binding,” *Physical Review Letters*, Vol. 63, No. 12, pp. 1233-1235, 1989.

33 T. M. Grzegorczyk, B. A. Kemp and J. A. Kong, “Passive guiding and sorting of small particles with optical binding forces,” *Optics Letters*, Vol. 31, No. 22, pp. 2278-3380, 2006.

34 Noack J, Vogel A: Laser-Induced Plasma Formation in Water at Nanosecond to Femtosecond Time Scales: Calculation of Thresholds, Absorption Coefficients, and Energy Density. IEEE J Quantum Elect 1999, 33(8): 1156-1167.

35 Vogel A, Noack J, Huttman G, Paltauf G: Mechanisms of femtosecond laser nanosurgery of cells and tissues. Appl Phys B 2005, 81: 1015-1047.

36 Schaffer CB, Brodeur A, Mazur E: Laser-induced breakdown and damage in bulk transparent materials induced by tightly focused femtosecond laser pulses. Meas Sci Technol 2001, 12: 1784-1794.

41 Kohli V, Elezzabi AY: Laser surgery of zebrafish (Danio rerio) embryos using femtosecond laser pulses: Optimal parameters for exogenous material delivery,

and the laser's effect on short- and long-term development. BMC Biotechnol 2008, 8)7): 1-20

42 Supatto W, Debarre D, Moulia B, Brouzes E, Martin JL, Farge E, Beaureparire E: In vivo modulation of morphogenetic movements in Drosophila embryos with femtosecond laser pulses. PNAS 2005, 102(4): 1047-1052.

37 M. Schumacher, S. Weill-Engerer, P. Liere, F. Robert, R. J. Franklin, L. M. Garcia-Segura, J. J. Lambert, W. Mayo, R. C. Melcangi, A. Parducz, U. Suter, C. Carelli, E. E. Baulieu, and Y. Akwa, "Steroid hormones and neurosteroids in normal and pathological aging of the nervous system," Prog Neurobiol*,* 71(1), 3-29 (2003).

38 J. L. Pawluski, S. Brummelte, C. K. Barha, T. M. Crozier, and L. A. Galea, "Effects of steroid hormones on neurogenesis in the hippocampus of the adult female rodent during the estrous cycle, pregnancy, lactation and aging," Front Neuroendocrinol*,* 30(3), 343-57 (2009).

39 J. W. Simpkins, J. Wang, X. Wang, E. Perez, L. Prokai, and J. A. Dykens, "Mitochondria play a central role in estrogen-induced neuroprotection," Curr Drug Targets CNS Neurol Disord*,* 4(1), 69-83 (2005).

40 D. L. Keefe, "Sex hormones and neural mechanisms," Arch Sex Behav*,* 31(5), 401-3 (2002).

44 J. M. Schwarz, S. L. Liang, S. M. Thompson, and M. M. McCarthy, "Estradiol induces hypothalamic dendritic spines by enhancing glutamate release: a mechanism for organizational sex differences," Neuron*,* 58(4), 584-98 (2008).

45 M. W. Berns, [A History of Laser Scissors (Microbeams)] Academic Press, (2007).

46 M. W. Berns, “Directed chromosome loss by laser microirradiation,” Science, 186(4165), 700-5 (1974).

47 M. W. Berns, J. Aist, J. Edwards, K. Strahs, J. Girton, P. McNeill, J. B. Rattner, M. Kitzes, M. Hammer-Wilson, L. H. Liaw, A. Siemens, M. Koonce, S. Peterson, S. Brenner, J. Burt, R. Walter, P. J. Bryant, D. van Dyk, J. Coulombe, T. Cahill, and G. S. Berns, “Laser microsurgery in cell and developmental biology,” Science, 213(4507), 505-13 (1981).

48 X. Kong, S. K. Mohanty, J. Stephens, J. T. Heale, V. Gomez-Godinez, L. Z. Shi, J. S. Kim, K. Yokomori, and M. W. Berns, “Comparative analysis of different laser systems to study cellular responses to DNA damage in mammalian cells,” Nucleic Acids Res, 37(9), e68 (2009).

49 E. Rieske, and G. W. Kreutzberg, “Neurite regeneration after cell surgery with laser microbeam irradiation,” Brain Res., 148(2), 478-483 (1978).

50 M. F. Yanik, H. Cinar, H. N. Cinar, A. D. Chisholm, Y. Jin, and A. Ben-Yakar, “Neurosurgery: functional regeneration after laser axotomy,” Nature, 432(7019), 822 (2004).

51 S. I. C. O. Santos, M. Mathew, and P. Loza-Alvarez, “Real time imaging of femtosecond laser induced nano-neurosurgery dynamics in C. elegans,” Opt. Express, 18(1), 364-377 (2010).

52 C. H. Tator, “Update on the Pathophysiology and Pathology of Acute Spinal Cord Injury,” Brain Pathology, 5(4), 407-413 (1995).

53 Bernhardt R, Axonal pathfinding during the regeneration of the goldfish optic pathway. J Comp Neurol, 1989 Jun 1; 284(1): 119-34

54 Stuermer CA, Bastmeyer M, Bahr M, et al., Trying to understand axonal regeneration in the CNS of fish, J Neurobiol 1992 Jul; 23(5): 537-50

55 M. F. Yanik, H. Cinar, H. N. Cinar, A. D. Chisholm, Y. Jin,A. Ben-Yakar, Functional regeneration after laser axotomy, Nature, 432 (2004).

56 G. Nageswara Rao, Sucheta S. Kulkarni, Sandhya P. Koushika and Kaustubh R. Rau, *In vivo* nanosecond laser axotomy: cavitation dynamics and vesicle transport, Opt. Exp. 16, 9884 (2008).

57 F. Bourgeois and A. Ben-Yakar, Femtosecond laser nanoaxotomy properties and their effect on axonal recovery in *C. elegans,* 9 15, Opt. Exp. 8521 (2007).

58 Landreth, G. E. & Agranoff, B. W. Explant Culture of Adult Goldfish Retina - Model for the Study of Cns Regeneration. *Brain Res* 161, 39-53 (1979).

59 Landreth, G. E. & Agranoff, B. W. Explant Culture of Adult Goldfish Retina - Effect of Prior Optic-Nerve Crush. *Brain Res* 118, 299-303 (1976).

60 Lemke, G, 2009 Developmental Neurobiology, Elsevier Inc., San Diego, CA pg 485

61 Thornton, J.E., Nock, B., McEwen, B.S., Feder, H.H., 1986. Estrogen induction of progestin receptors in microdissected hypo- thalamic and limbic nuclei of female guinea pigs. Neuroendocrinology 43, 182±188.

62 Blaustein, J.D., King, J.C., Toft, D.O., Turcotte, J., 1988. Immunocytochemical localization of estrogen-induced progestin receptors in guinea pig brain. Brain Res. 474, 1±15.

63 DonCarlos, L.L., Greene, G.L., Morrell, J.I., 1989. Estrogen plus progesterone increases progestin receptor immunoreactivity in the brain of ovariectomized guinea pigs. Neuroendocrinology 50, 613±623.

64 Naftolin, F., 1994. Brain aromatization of androgens. J. Reprod. Med. 39, 257±261.

65 Hutchison, J.B., Wozniak, A., Beyer, C., Karolczak, M., Hutchison, R.E., 1999. Steroid metabolising enzymes in the determination of brain gender. J. Steroid Biochem. Mol. Biol. 69, 85±96.

66 J. W. Simpkins, P. S. Green, K. E. Gridley, M. Singh, N. C. de Fiebre, and G. Rajakumar, “Role of estrogen replacement therapy in memory enhancement and the prevention of neuronal loss associated with Alzheimer's disease,” Am J Med, 103(3A), 19S-25S (1997).

67 M. Singh, E. M. Meyer, and J. W. Simpkins, “The effect of ovariectomy and estradiol replacement on brain-derived neurotrophic factor messenger ribonucleic acid expression in cortical and hippocampal brain regions of female Sprague-Dawley rats,” Endocrinology, 136(5), 2320-4 (1995).

68 E. J. Huang, and L. F. Reichardt, “Neurotrophins: roles in neuronal development and function,” Annu Rev Neurosci, 24, 677-736 (2001).

69 M. Schumacher, S. Weill-Engerer, P. Liere, F. Robert, R. J. Franklin, L. M. Garcia-Segura, J. J. Lambert, W. Mayo, R. C. Melcangi, A. Parducz, U. Suter, C. Carelli, E. E. Baulieu, and Y. Akwa, “Steroid hormones and neurosteroids in normal and pathological aging of the nervous system,” Prog Neurobiol, 71(1), 3-29 (2003).

70 J. L. Pawluski, S. Brummelte, C. K. Barha, T. M. Crozier, and L. A. Galea, “Effects of steroid hormones on neurogenesis in the hippocampus of the adult female rodent during the estrous cycle, pregnancy, lactation and aging,” Front Neuroendocrinol, 30(3), 343-57 (2009).

71 J. W. Simpkins, J. Wang, X. Wang, E. Perez, L. Prokai, and J. A. Dykens, “Mitochondria play a central role in estrogen-induced neuroprotection,” Curr Drug Targets CNS Neurol Disord, 4(1), 69-83 (2005).

72 Mueller, B. K. Growth cone guidance: First steps towards a deeper understanding. *Annu Rev Neurosci* 22, 351-388 (1999).

73 Lowery, L. A. & Van Vactor, D. The trip of the tip: understanding the growth cone machinery. *Nat Rev Mol Cell Bio* 10, 332-343, doi:Doi 10.1038/Nrm2679 (2009).

74 Chedotal, A. & Richards, L. J. Wiring the Brain: The Biology of Neuronal Guidance. *Csh Perspect Biol* 2, DOI 10.1101/cshperspect.a001917 (2010).

75 Pittman, A. J., Law, M. Y. & Chien, C. B. Pathfinding in a large vertebrate axon tract: isotypic interactions guide retinotectal axons at multiple choice points. *Development* 135, 2865-2871, doi:Doi 10.1242/Dev.025049 (2008).

76 Erskine, L. & Herrera, E. The retinal ganglion cell axon's journey: Insights into molecular mechanisms of axon guidance. *Dev Biol* 308, 1-14, doi:DOI 10.1016/j.ydbio.2007.05.013 (2007).

77 Harrelson, A. L. Molecular Mechanisms of Axon Guidance in the Developing Insect Nervous-System. *J Exp Zool* 261, 310-321 (1992).

78 Inatani, M. Molecular mechanisms of optic axon guidance. *Naturwissenschaften* 92, 549-561, doi:DOI 10.1007/s00114-005-0042-5 (2005).

79 Fawcett, J. Repair of spinal cord injuries: where are we, where are we going? *Spinal Cord* 40, 615-623, doi:DOI 10.1038/sj.sc.3101328 (2002).

80 Zeck, G. & Fromherz, P. Noninvasive neuroelectronic interfacing with synaptically connected snail neurons immobilized on a semiconductor chip. *P Natl Acad Sci USA* 98, 10457-10462 (2001).

81 Fromherz, P. Three levels of neuroelectronic interfacing - Silicon chips with ion channels, nerve cells, and brain tissue. *Ann Ny Acad Sci* 1093, 143-160, doi:DOI 10.1196/annals.1382.011 (2006).

82 Mai, J., Fok, L., Gao, H. F., Zhang, X. & Poo, M. M. Axon Initiation and Growth Cone Turning on Bound Protein Gradients. *J Neurosci* 29, 7450-7458, doi:Doi 10.1523/Jneurosci.1121-09.2009 (2009).

83 Yu, T. W. & Bargmann, C. I. Dynamic regulation of axon guidance. *Nat Neurosci* 4, 1169-1176 (2001).

84 Borisy, G. G. & Svitkina, T. M. Actin machinery: pushing the envelope. *Curr Opin Cell Biol* 12, 104-112 (2000).

85 Dickson, B. J. Molecular mechanisms of axon guidance. *Science* 298, 1959-1964 (2002).

86 Ming, G. L. *et al.* Adaptation in the chemotactic guidance of nerve growth cones. *Nature* 417, 411-418 (2002).

87 Hoffman-Kim, D., Mitchel, J. A. & Bellamkonda, R. V. Topography, Cell Response, and Nerve Regeneration. *Annu Rev Biomed Eng* 12, 203-231, doi:DOI 10.1146/annurev-bioeng-070909-105351 (2010).

88 Patel, N. & Poo, M. M. Orientation of Neurite Growth by Extracellular Electric-Fields. *J Neurosci* 2, 483-496 (1982).

89 Blau, A. *et al.* Promotion of neural cell adhesion by electrochemically generated and functionalized polymer films. *J Neurosci Meth* 112, 65-73 (2001).

90 Wu, T. *et al.* A photon-driven micromotor can direct nerve fibre growth. *Nature Photonics* 6, 62-67, doi:Doi 10.1038/Nphoton.2011.287 (2012).

91 Luo, Y. & Shoichet, M. S. A photolabile hydrogel for guided three-dimensional cell growth and migration. *Nat Mater* 3, 249-253, doi:Doi 10.1038/Nmat1092 (2004).

92 Ehrlicher, A. *et al.* Guiding neuronal growth with light. *P Natl Acad Sci USA* 99, 16024-16028, doi:DOI 10.1073/pnas.252631899 (2002).

93 Mohanty, S. K., Sharma, M., Panicker, M. M. & Gupta, P. K. Controlled induction, enhancement, and guidance of neuronal growth cones by use of line optical tweezers. *Opt Lett* 30, 2596-2598 (2005).

94 Mathew, M. *et al.* Signalling effect of NIR pulsed lasers on axonal growth. *J Neurosci Meth* 186, 196-201, doi:DOI 10.1016/j.jneumeth.2009.11.018 (2010).

95 Wu, T. *et al.* Neuronal growth cones respond to laser-induced axonal damage. *Journal of The Royal Society Interface* 9, 535-547, doi:DOI 10.1098/rsif.2011.0351 (2012).

96 Gittes, F., Mickey, B., Nettleton, J. & Howard, J. Flexural Rigidity of Microtubules and Actin-Filaments Measured from Thermal Fluctuations in Shape. *J Cell Biol* 120, 923-934 (1993).

97 Ashkin, A., Dziedzic, J. M., Bjorkholm, J. E. & Chu, S. Observation of a Single-Beam Gradient Force Optical Trap for Dielectric Particles. *Opt Lett* 11, 288-290 (1986).

98 Sachs, F. Stretch-Activated Ion Channels: What Are They? *Physiology* 25, 50-56, doi:DOI 10.1152/physiol.00042.2009 (2010).

99 Sachs, F. Mechanical Transduction by Membrane Ion Channels - a Mini Review. *Mol Cell Biochem* 104, 57-60 (1991).

100 Gomez, T. M. & Spitzer, N. C. Regulation of growth cone behavior by calcium: new dynamics to earlier perspectives. *J Neurobiol* 44, 174-183 (2000).

101 Harada, Y. & Asakura, T. Radiation forces on a dielectric sphere in the Rayleigh scattering regime. *Opt Commun* 124, 529-541 (1996).

102 Liu, Y. *et al.* Evidence for Localized Cell Heating Induced by Infrared Optical Tweezers. *Biophysical journal* 68, 2137-2144 (1995).

103 Niranjan, P. S. *et al.* The polymerization of actin: Thermodynamics near the polymerization line. *J Chem Phys* 119, 4070-4084, doi:Doi 10.1063/1.1592499 (2003).

104 Henley, J. & Poo, M. Guiding neuronal growth cones using Ca2+ signals. *Trends Cell Biol* 14, 320-330 (2004).

105 Wang, G. X. & Poo, M. M. Requirement of TRPC channels in netrin-1-induced chemotropic turning of nerve growth cones. *Nature* 434, 898-904, doi:Doi 10.1038/Nature03478 (2005).

106 Fohlmeister, J. F., Cohen, E. D. & Newman, E. A. Mechanisms and Distribution of Ion Channels in Retinal Ganglion Cells: Using Temperature as an Independent Variable. *J Neurophysiol* 103, 1357-1374, doi:DOI 10.1152/jn.00123.2009 (2010).

107 Sappington, R. M., Sidorova, T., Long, D. J. & Calkins, D. J. TRPV1: Contribution to Retinal Ganglion Cell Apoptosis and Increased Intracellular Ca(2+) with Exposure to Hydrostatic Pressure. *Invest Ophth Vis Sci* 50, 717-728, doi:Doi 10.1167/Iovs.08-2321 (2009).

108 Talavera, K., Nilius, B. & Voets, T. Neuronal TRP channels: thermometers, pathfinders and life-savers. *Trends Neurosci* 31, 287-295, doi:DOI 10.1016/j.tins.2008.03.002 (2008).

109 Sihvola, AH, Electromagnetic mixing formulas and applications, The Institution of Electrical Engineers, London, U.K., 1999, pg. 228.

110 Venermo, J, Sihvola, Ari, Dielectric polarizability of circular cylinder, Journal of Electrostatics 63 (2005) 101-117

Biographical Information

Bryan Black's academic career began at Cape Fear Community College, in Wilmington, N.C., during the spring of 2007. After completing most of his basic studies requirements, he transferred to the University of North Carolina at Wilmington, where he earned merit scholarships, Dean's list honors all four semesters of residence, and the Marvin Moss award for study in the field of science. Bryan graduated from UNCW with a B.S. in physics in the spring of 2010, and was admitted to the department of physics at the University of Texas at Arlington for the following fall. Bryan plans on completing his Master of science degree in physics in the fall of 2012, and will continue with his graduate work in pursuit of his Ph.D. in Physics. His research interests include the application of light in the manipulation of objects in the micro-regime, single motor molecule dynamics, and neuron guidance. Bryan plans to graduate with his terminal degree in physics in the spring of 2014, after which he will apply for post-doctoral positions.